SHRP-ID/UFR-90-002

A Low-Cost Fiber Optic Weigh-In-Motion Sensor

Ahmad Safaai-Jazi
Virginia Polytechnic Institute and State University

Siamak A. Ardekani
The University of Texas

Majid Mehdikhani
Virginia Polytechnic Institute and State University

Strategic Highway Research Program
National Research Council
Washington, DC 1990

SHRP–ID/UFR-90-002
Contract ID013

Program Manager: *K. Thirumalai*
Program Area Secretary: *Francine Burgess*

Reprint November 1993
November 1990

key words:
fiber-optic weigh-in-motion sensor
fiber optics
highway data collection
traffic data collection
vehicle weight
weight data collection
weigh-in-motion sensors

Strategic Highway Research Program
National Academy of Sciences
2101 Constitution Avenue N.W.
Washington, DC 20418

(202) 334-3774

50/NAP/1193

Contents

Acknowledgements

The research herein described was supported by the Strategic Highway Research Program (SHRP). SHRP is a unit of the National Research Council that was authorized by section 128 of the Surface Transportation and Uniform Relocation Assistance Act of 1987.

The authors would like to thank Ahmad Rasvan of the Engineering Science and Mechanics Department, Virginia Polytechnic Institute and State University (VPI&SU), for his assistance in conducting the Material Test Systems (MTS) tests, and Riley Chan of the Chemical Engineering Department, VPI&SU, for manufacturing the pneumatic tubes. Thanks also are expressed to Dr. Mohsen Kashi and Dr. Richard Weyers of the Civil Engineering Department, VPI&SU, for their discussions and suggestions.

The financial support of this research by SHRP under contract SHRP-89-ID013 is gratefully acknowledged.

Abstract

Automated techniques designed to acquire weight and traffic data are indispensable to the effective management of the nation's vast network of highways. Weigh-In-Motion (WIM) systems have the potential to reduce the cost and improve the accuracy associated with weight data collection. The existing WIM systems utilizing piezoelectric cable have been shown to result in significant errors and to require in-pavement installation.

A fiber-optic WIM sensor, which offers several advantages over the piezoelectric sensor, is proposed. The system consists of a pneumatic tube filled with an incompressible fluid and embedded in a rubber pad, a diaphragm designed to convert pressure into displacement, and an optical displacement sensor. A prototype of the proposed sensor is designed, manufactured, and tested in the laboratory for different load-frequency combinations using an MTS machine. Statistical analyses of data are performed to assess the response of the sensor under varying load frequencies.

A piezoelectric cable also is tested under varying load frequencies for the purpose of comparison with the proposed sensor. It is shown that the piezoelectric cable sensor exhibits considerable dependence on the load frequency; whereas, the response of the proposed sensor is much less frequency-dependent and, unlike the piezoelectric cable, has a waveform similar to that of the applied load. This latter property can facilitate significantly the processing of the sensor output signal. The linearity of response over the range of applied loads also is better than that of the piezoelectric cable.

Finally, the proposed sensor is not susceptible to electromagnetic interference (EMI), is less expensive, and can be installed on the surface of the pavement, thus eliminating the need to dig the pavement.

Executive Summary

WIM systems are of considerable interest to the traffic control and the management of the vast network of highways in the nation. The existing technologies for WIM, utilizing strain gauges or piezoelectric cables, are either too expensive, or do not provide weight date with sufficient accuracy.

In an effort to reduce the cost and improve the accuracy associated with weight-data collection, a new concept for weighing-in-motion, based on fiber-optic technology, was proposed to SHRP and was approved for a Phase I study. This summary describes the highlights of the research and the accomplishments in Phase I of this SHRP-IDEA project.

Research Accomplishments

The feasibility of a fiber-optic WIM sensor was studied. The research work involved the development of a prototype optical pressure sensor, laboratory tests with a MTS (Material Test Systems) machine to study the sensor response under different loads and at different frequencies, analysis and testing of the significance of data, and comparison with the piezoelectric sensor.

Design and Fabrication of the Sensor

The essential elements of the proposed fiber-optic WIM sensor are a pneumatic tube filled with an incompressible fluid, a diaphragm to convert pressure into displacement, and an optical displacement sensor.

The tube is an expandable hose with an inner diameter of 0.25 inches. It is housed in a rubber pad which serves as a mechanical support. The tube is connected at both ends to flexible, but nonexpandable, stainless-steel hoses and is filled with an incompressible fluid.

The stainless-steel diaphragm is placed at one end of the pneumatic tube between the optical displacement sensor and the flexible steel hose. The applied pressure causes the diaphragm to deflect. One side of the diaphragm is attached to a light-blocking element which serves as a spatial light modulator. Pressure changes experienced by the pneumatic tube are ultimately converted into variations in light intensity.

Two fiber-optic displacement sensors based on intensity modulation of light were designed and evaluated. Both sensors were studied in the laboratory using a micropositioner to simulate the deflection of the diaphragm. The use of gratings to increase sensitivity was also investigated.

The rubber pad is used primarily for mechanical support and to transmit evenly the applied pressure to the encased expandable tube. The material composition of the pad is resin, a softening agent and curing agent. The hardness of the pad plays an important role in transmitting the pressure from a vehicle to the expandable tube, thus affecting the magnitude of the sensor-output signal and requiring calibration.

Two steel hoses, one 6 feet long and another 1 foot long, are used. The function of the longer steel hose is to transmit the pressure from the load region to the diaphragm with minimal loss; whereas, the shorter steel hose is used to facilitate the removal of trapped air bubbles. Two air-bleed valves, one at each end of the sensor assembly, are used to remove trapped air in the fluid-filled part of the system.

Laboratory Tests and Performance Evaluation of the Sensor

The fabricated sensor was tested using a 20-Kip MTS machine to simulate different vehicle weights and speeds. The rubber pad was mounted onto the stationary upper plate of the MTS machine. Load was applied from underneath through a metallic support plate. Ten levels of loads, from 1 Kip to 5.5 Kips in 0.6 Kip increments were applied. Each load was applied at frequencies of 0.25, 0.5, 1.0, 2.0, 5.0, and 10.0 Hz. Several cycles of a square wave were applied for each load-frequency combination. The input and output waveforms were monitored simultaneously, using a dual channel oscilloscope, and photographed following each load application. Examination of the output waveforms revealed an interesting feature: for square wave input waveforms, the output waveforms were also square wave. This property of the optical sensor is a major advantage over the piezoelectric sensor and will be very useful in processing the output signal and in correlating it to the weight of the vehicle.

The measured output signal voltages suggest that in the frequency range 0.25 Hz through 10.0 Hz the sensor response is largely frequency-independent. To assess the behavior of the sensor response quantitatively, the output voltage versus the applied load was plotted for six different frequencies. Furthermore, statistical tests were performed on the data to determine the level of significance (*p-values*) and the coefficient of determination (R^2) as measures of frequency independence and linearity of the sensor response, respectively. The independence of the sensor output signal from frequency implies the accurate measurement of weights at different vehicle speeds.

An important attribute of the sensor response is the correlation between the applied load and the output-signal voltage. The best-fit regression line through the data points was obtained. The coefficient of determination, R^2, is 99.5%, indicating a practically linear relation between the applied load and the output signal.

Similar laboratory tests and data analysis were performed on a piezoelectric sensor for the purpose of comparison with the proposed optical sensor.

Significance of Results and Comparison with Piezoelectric Cable

Shape, linearity, and variations with frequency of the output signal have a direct bearing on the accuracy of a WIM sensor. In terms of the shape of the output signal, the piezoelectric cable generated exponentially decaying output waveforms for square wave inputs. In other words, the optical sensor reported a constant voltage reading as long as the MTS loading cell was in contact with the sensor. On the contrary, the piezoelectric sensor output signal peaks to a maximum value upon the application of the load and decreases exponentially with time. In processing the WIM sensor output signals, the area underneath the output signal is an important factor in determining the axle weights. Therefore, square wave output signals of the fiber-optic sensor offer a major advantage over the exponentially decaying output signals of the piezoelectric cable.

Another advantage of the fiber-optic sensor is that of output signal variations with load frequency. Comparison of output waveforms as well as the output voltage-load curves for the optical and piezoelectric sensors indicate that the signal outputs vary considerably less with load frequency in the case of the fiber-optic sensor. Ideally, the response of a WIM sensor should be entirely frequency-independent. The stronger frequency dependence of the piezoelectric output signal in both the shape of the waveform and the peak voltage implies that the speed and axle spacing of vehicles could be a serious source of error in piezoelectric WIM sensors, but not in the proposed fiber-optic WIM sensors. The linearity of the output voltage with load for both optical and piezoelectric sensors is satisfactory.

In short, both the output waveform and the lack of strong frequency dependence in the fiber-optic sensor output signals contribute significantly to higher accuracies. In addition, the fiber-optic signal can be made immune to EMI. Furthermore, unlike the piezoelectric case, the electronic components in the optical sensor are not in direct contact with the wheel. Finally, the optical sensors can be made temperature-insensitive. However, the bending characteristics of the piezoelectric sensors have been shown to change at high temperatures encountered in the roadside environment.

The optical sensors also offer a considerably lower life-cycle cost. They are portable and are installed on the pavement surface. As such, they can be installed rapidly and with minimal traffic interruption, especially since there is no need to dig the pavement and embed the sensor, or to affix it to the surface. The electronic components of the optical sensor are cheaper and readily available because they are mass-produced for a variety of other applications in the fiber-optics and communications fields. The electronic and optical components of the sensor, which comprise a major fraction of the total sensor cost (over 60 percent) cost under $600 per sensor unit at the time of writing this report. Furthermore, the electronic and optical components are installed on the side of the road, or even housed in a remote location, and would never be in contact with the traffic, thus lasting longer. The above-mentioned attributes contribute to a lower life-cycle cost of the optical sensor as compared with other conventional WIM sensors in use today.

1

Background Information and Technical Approach

Overview

To properly plan for the maintenance and management of the nation's vast network of highways, large quantities of traffic data are required. At minimum, data must be collected on the number, type, weight, and speed of vehicles on the highways. To date, the need exists for automated techniques to acquire such data economically and accurately. Currently, for example, most truck weight data are obtained statically at truck weigh stations. These facilities are not only costly to equip and operate, but are also fixed in location and, often operating hours. Consequently, the weight data obtained tend to underestimate the number of over-weight trucks that manage to bypass the stations.

In this regard, WIM systems have the great potential to reduce the cost and improve the accuracy associated with weight data collection. Early WIM systems generally consisted of a number of strain gauges mounted on the underside of bridge girders, or under flush-type platforms. The major drawback of such systems has been their high cost, typically ranging from $50,000 to $200,000 per unit.

Almost from the inception of WIM systems in the early 1950s, efforts have been concentrated on developing low-cost WIM sensors. As part of these efforts, the use of piezoelectric cables has reduced subsequently the equipment cost. For example, the states of Iowa and Minnesota have each installed a piezoelectric WIM system for an approximate equipment cost of $5000 per lane [1]. Colorado [2] and Texas [3,4] have experimented also with this technology.

Despite their relatively low cost and small systematic errors, piezoelectric

sensors have been shown to result in rather large random errors for individual axles. Researchers in Canada reported piezoelectric cable accuracy of 6% to 12% as compared to the dynamic axle load measurements by an instrumented vehicle [5]. The experiments in Canada involved three vehicle speeds, two levels of tire pressure, and two suspension types. Studies in Texas involving some 800 trucks, weighed both statically and by using the piezoelectric WIM system, showed overall random errors of up to 9% [6]. Studies in Iowa involving 456 trucks reported overall random errors of up to 12% [7] for a WIM system installed in a rigid (portland concrete) pavement. Similar experiments designed for a flexible (asphalt concrete) pavement case in Minnesota were not performed due to problems relating to the sensor installation, electronics and pavement behavior [7].

Although installation problems such as those encountered in Minnesota can eventually be resolved, the magnitude of random errors in other performed studies is rather large. Such errors are attributed to the internal geometry and bending characteristics of the cable, the design of sensor mounting, and the roadway surface profile upstream of sensor installation [8].

The use of a fiber-optic sensor is highly promising as a replacement for the piezoelectric cable in WIM systems. Fiber-optic sensors have the potential to alleviate a number of error sources associated with the piezoelectric sensors. Furthermore, they offer potentially lower equipment, installation, and maintenance cost.

Fiber-optic sensing techniques have attracted considerable attention in recent years. Among the various advantages offered by fiber-optic sensors, the low cost, high accuracy, and immunity from EMI are particularly appealing to vehicle weighing and traffic control applications.

An inductive pickup provides a large output signal and is less expensive than a fiber optic sensor. It is, however, susceptible to EMI and is not recommended for the WIM application.

Approach

In fact, the main problem of vehicle weighing is pressure sensing. Various techniques for pressure sensing using fiber-optic technology have been studied in the past decade [9-13]. These techniques are based on variations of one or more of transmission properties of the light. The simplest pressure sensor operates on the basis of amplitude modulation of the light. Amplitude sensors are easy to construct, inexpensive, and function reliably in harsh environments. For applications where moderate sensitivities are sufficient, amplitude sensors are suitable candidates. In situations where high sensitivities are required, Mach-Zehnder interferometric phase sensors may be utilized [14]. Phase sensors, however, have complicated structures and are expensive. Another promising pressure sensor is based on modal inter-

ference in a few-mode fiber which offers sensitivities between those of amplitude and phase sensors [15].

For vehicle weighing applications, an amplitude sensor is a reasonable choice because it is low cost and can offer the desired accuracy. An important advantage of amplitude sensors is that the power is much less sensitive to random temperature variations than the phase sensors. This aspect is of considerable importance in designing reliable optical WIM sensors. Fiber-optic pressure sensing can be implemented using a variety of techniques. The sensing mechanism may be either intrinsic ,in which case, the pressure affects the fiber directly, or extrinsic where the modulation of light takes place outside the fiber. Here an extrinsic approach is adopted. The pressure generated by the weight of a vehicle upon passing over a fluid-filled pneumatic tube is converted to displacement by means of a diaphragm. The deflection of diaphragm modulates the light.

A prototype pressure sensor, operating based on an extrinsic fiber-optic displacement sensing technique, is designed, analyzed, and evaluated experimentally. Fiber-optic techniques for pressure sensing are addressed in Chapter 2. Advantages and disadvantages of various techniques are pointed out and ways of improving the sensitivity are discussed. Design and manufacturing of the proposed sensor are addressed in Chapter 3. Mechanical design considerations, experimental results, and evaluation of the performance of the proposed sensor are discussed in Chapter 4. Laboratory tests on piezoelectric sensor and comparison with the optical sensor are addressed in Chapter 5. Concluding remarks and suggestions for further work are summarized in Chapter 6.

2

Fiber-Optic Techniques for Pressure Sensing

This chapter examines various fiber- optic techniques for the measurement of pressure. The principles of operation of fiber-optic pressure sensors are discussed. Sensing techniques based on the modulation of amplitude or phase of light are addressed. Both intrinsic and extrinsic sensing mechanisms are reviewed. Various options pertinent to WIM systems are evaluated, and a design is proposed taking into account cost, accuracy, and durability of the sensor.

Principles of Operation

A light beam is associated with a number of physical properties including amplitude (intensity), phase, wavelength (color), polarization, and mode of propagation. In the absence of any external disturbance, the properties of light remain unchanged. If an external disturbance such as pressure, stress, strain, temperature, electric field, etc., perturbs the transmission medium in some way, one or more properties of the light will change. The amount of change is a measure of the external disturbance.

In this work, the external disturbance is the pressure generated by the weight of a vehicle. Pressure can perturb the transmission medium in many different ways. If the transmission medium in contact with the pressure region is an optical fiber, perturbations would commonly include bends, microbends, refractive index change, induced anisotropy, and dimensional changes, all of which affect the transmission properties of the light propagating in the fiber. Geometrical changes such as bends and microbends affect the intensity considerably; whereas, perturbations in the refractive index bring about significant changes in the phase. The loss of power resulting from bends and microbends is due to the conversion of the guided modes to radiation modes. Variations of the phase, on the other hand, result from

the elasto-optic effect as well as changes in the fiber dimensions.

When the transmission medium is air, the disturbance can alter indirectly the properties of light. For example, pressure can move a blocking element, and cause the light to be only partially transmitted. Variations in the transmitted or reflected power are related then to the applied pressure.

Intrinsic Sensing Techniques

As discussed earlier, the parameters specifying the light propagating in an optical fiber can be altered if the fiber is subjected directly to external perturbations such as pressure, strain, etc. These changes can then be correlated to the measurand of interest. Optical sensing techniques are further subdivided into two categories; each category operates on substantially different principles and areas of application. Both categories include sensors which operate based on the transmission or reflection losses. For the first group, the intensity pattern by the light launched into the fiber is altered due to the direct application of the physical quantity to be measured (intrinsic).

Often it is desired to acquire information about a parameter of interest, such as pressure, and to transmit the information to a convenient location due to the nature of application, or the environmental set of conditions imposed. This concept makes up the characteristic feature of the second group. In the latter group, modulation of light is correlated to the measurand indirectly (extrinsic). For example, pressure can be converted into displacement which, in turn, can change the power of a reflected or transmitted light. This concept is the basis of the optical sensing technique employed for WIM and is further elaborated upon in later sections.

Amplitude Sensing Technique

This technique is based on the idea that the external disturbance modulates the insertion loss of the optical fiber. If two corrugated plates, known as deformers, sandwich an optical fiber along its axis as shown in Fig. 2-1, and the plates are displaced with respect to one another due to the introduction of an external pressure, a spatial periodic fiber deformation will be developed. This deformation, in turn, will cause mode coupling. Light is redistributed among newly developed modes, and, at the same time, power is coupled from guided modes to radiation modes. The amount of power coupled to radiation modes which escapes the fiber is an excess loss. It has been shown [16] that for microbend deformations, mode coupling of light occurs between every two modes whose propagation constants K_1 and K_2 satisfy the condition $K_1 - K_2 = \pm (2\pi/\Lambda)$, where Λ is the mechanical wavelength of the periodic microbend disturbance. By closely monitoring the optical power at the output end of the fiber, one can determine the amount of the applied pressure. Microbend sensors offer sufficient sensitivities and are suitable candidates for the measurements of relatively small pres-

sures. Since optical fibers cannot sustain high shear stresses, microbend sensors are not favored for WIM applications.

Interferometric Sensing Technique

This technique incorporates the phase modulation of optical signal to measure the external disturbance. It can be implemented using a variety of schemes. An arrangement commonly used in fiber-optic sensing is the Mach-Zehnder interferometer shown schematically in Fig. 2-2. This interferometer consists of essentially two arms, one serving as sensing arm and another as reference arm. The light signal is divided between the two arms using a 3-dB coupler. The external disturbance affects only the sensing arm and causes the light signal propagating in this arm to undergo a phase change. The signals of the two arms are then combined using a second 3-dB coupler. The two signals interfere, and, as a result the phase difference between them is converted to an amplitude change, which can be easily monitored and measured by means of a detection circuit.

Interferometric sensors offer very high sensitivities and are useful for measuring very small disturbances. A major drawback of these sensors is their sensitivity to random temperature variations. To eliminate this problem, sophisticated control systems are required, which make the sensor complicated and expensive. As in WIM systems pressures are not small and the cost must be minimized, an interferometric type sensor is not a suitable choice.

Extrinsic Sensing Techniques

In an extrinsic fiber-optic sensing scheme, the external disturbance does not affect the fiber directly. That is, the light is modulated outside the fiber. The role of the fiber in such sensors is to transmit light to and from the sensing region. Extrinsic fiber-optic sensors are of particular interest in low-cost WIM systems. Here two sensing schemes based on reflection and transmission of light are described.

Reflection-Based Method

Fig. 2-3 illustrates the schematic diagram of a pressure sensor based on the external modulation of light intensity. Light is coupled into a multimode fiber from an LED (Light Emitting Diode) or a diode laser. The length of the fiber depends upon the need for a specific application. The fiber is followed by a 3-dB coupler which divides the power into halves. One of the coupler's output fiber is attached to a GRIN (Graded-Index) lens which collimates and expands the light beam, while the other output fiber is immersed in an index matching fluid which absorbs the light. Parallel to the GRIN lens face, a mirror is mounted which can move vertically. The motion of the mirror is controlled by the pressure to be measured. In the absence of any pressure, the mirror does

not block the light exiting the GRIN lens, thus no reflection takes place. By increasing the pressure, the mirror is displaced in the vertical direction, thus causing a portion of light to be reflected back into the GRIN lens. The reflected light is focused (by the GRIN lens) on to the fiber, passes through the coupler, and half of its power eventually reaches the detector. The detector's output voltage is proportional to the reflected power, which, in turn, is dependent upon the applied pressure. The GRIN lens helps the system to respond more linearly by collimating the light beam.

Transmission-Based Method

In the reflection-based scheme described above, twice the power is divided into halves, effecting a 6-dB loss. Besides, the fiber-GRIN lens connection needs very careful alignment to avoid further loss of power. The power efficiency can be improved by a factor of 6-dB by eliminating the coupler and using a separate channel for the detector, as illustrated in Fig. 2-4. The principle of operation of this sensor is the same as that of Fig. 2-3; however, the detector measures the power of the transmitted light. If the sensing region can accommodate the source, the detector, and associated electronics, fibers and GRIN lenses may also be eliminated, and the sensor head assembly reduces to that shown in Fig. 2-5.

Use of Gratings to Increase Sensitivity

Gratings can be used to increase sensitivity for both reflection-based and transmission-based sensors. Here the use of gratings in transmission-based sensors is described. Gratings are parallel and equally spaced strips deposited on transparent glass substrates or mirrors as shown in Fig. 2-6a.

The material used in the construction of gratings should be highly absorptive (e.g., black). One grating is placed in front of the GRIN lens (or LED if GRIN lens is not used), and another one replaces the blocking element in Fig. 2-5. When the strips of the gratings overlap completely, maximum transmission takes place (Fig. 2-6b). When the grating attached to the diaphragm is displaced, the path of light is partially blocked and transmission is reduced (Fig. 2-6c). For a displacement equal to one half the grating period, the path is completely blocked and transmission is reduced to zero (Fig. 2-6d). This qualitative analysis, of course, does not take into account the diffraction of light by the strips edges. Obviously, the sensitivity can be increased by reducing the grating period. It should be noted that, the response of the sensor becomes periodic, and there is a 3-dB power loss, because, in the absence of any displacement when the gratings are assumed to have a perfect overlap, only half the power is transmitted.

In summary, the relative merits of several sensing techniques have been evaluated and compared. The sensing

techniques studied here, are seen to offer different accuracies, power consumption, and parts count. As the feasibility of developing a low-cost WIM sensor as a possible replacement for the presently implemented piezoelectric WIM sensor was the objective of this research, then designs based on transmission-based sensing techniques are justified. They are relatively low-cost, and all the optical and associated electronic components can be packaged in a small unit.

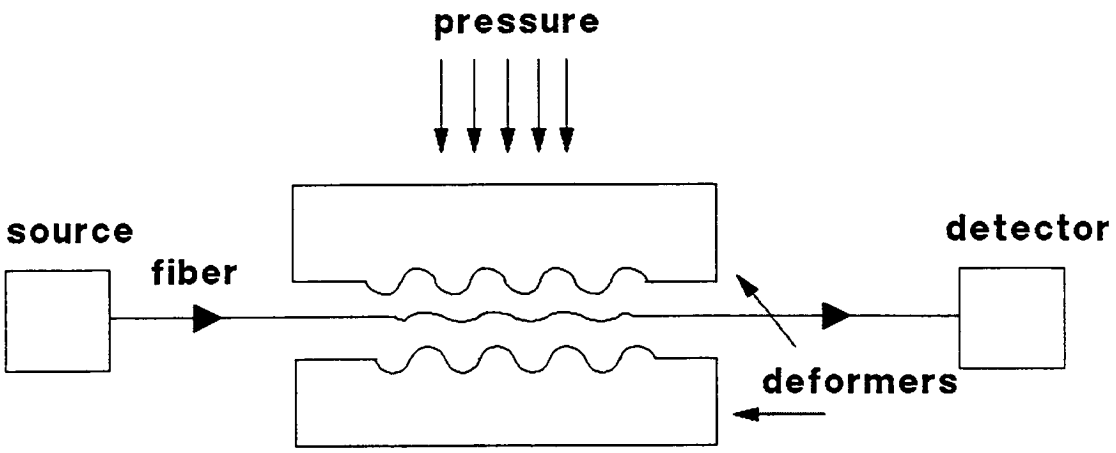

Fig. 2-1 Schematic diagram of microbend sensor.

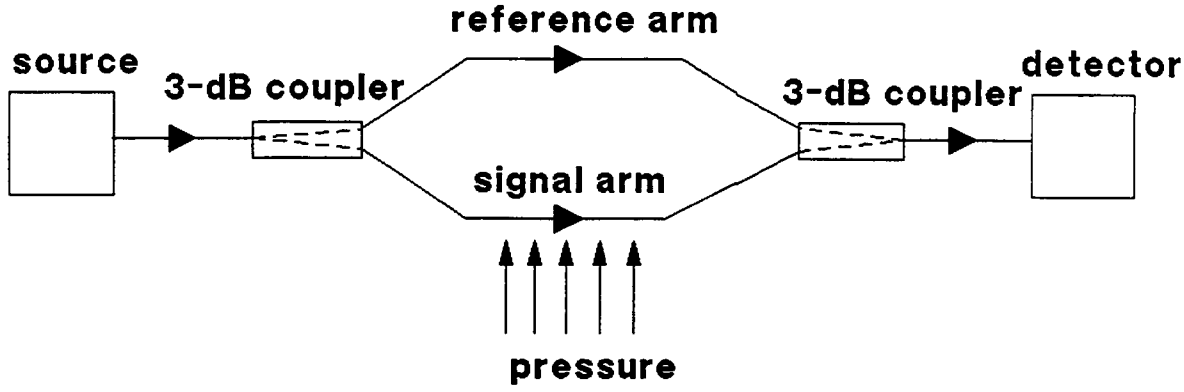

Fig. 2-2 Schematic diagram of a Mach-Zehnder interferometric sensor.

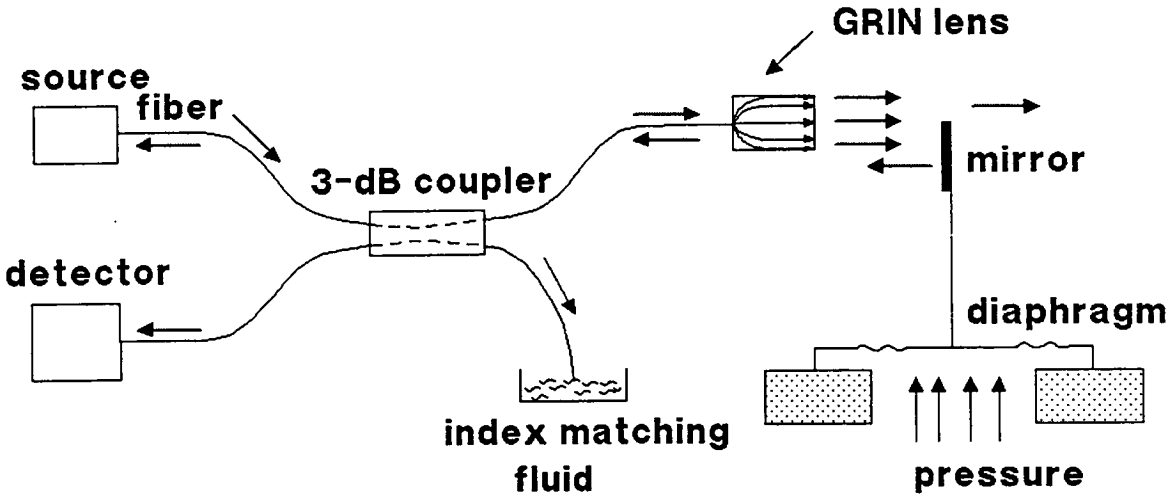

Fig. 2-3 Schematic diagram of a reflection-based pressure sensor.

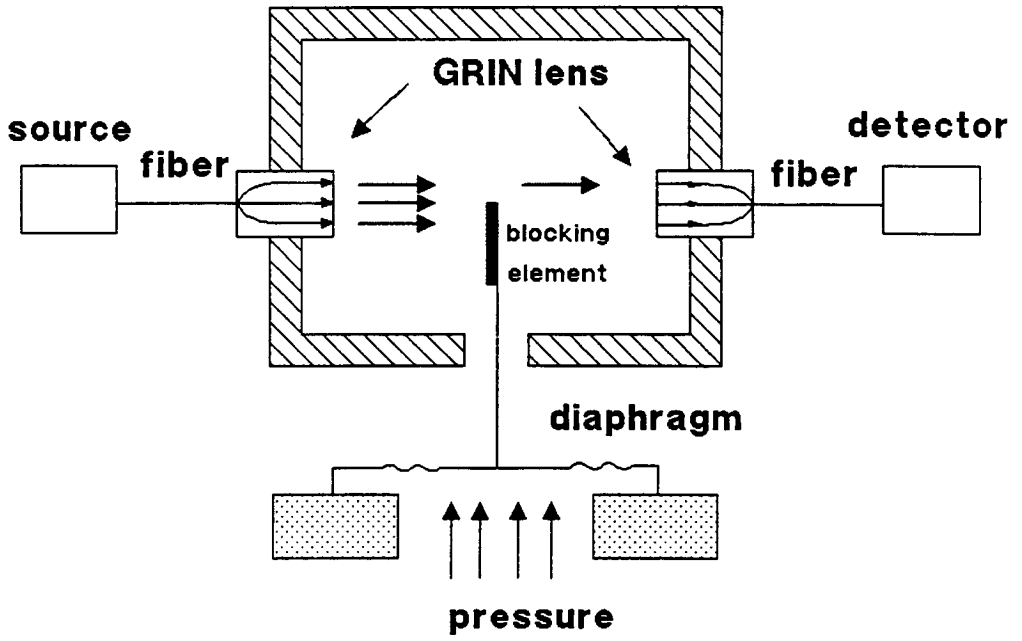

Fig. 2-4 Schematic diagram of a transmission-based pressure sensor.

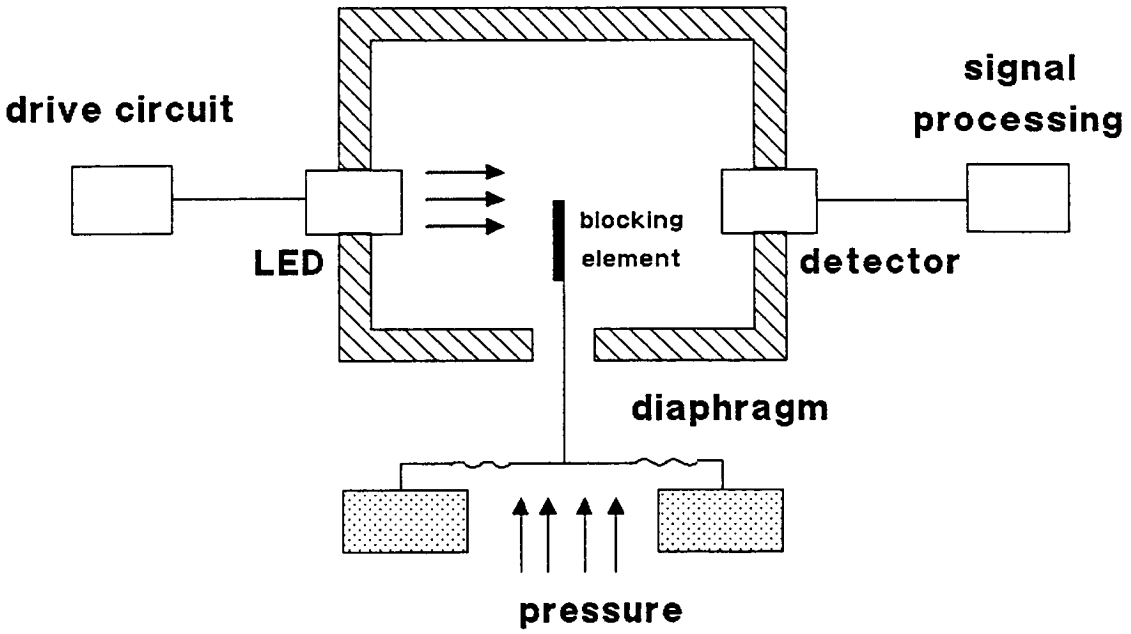

Fig. 2-5 Modified transmission-based pressure sensor without fiber and GRIN lens.

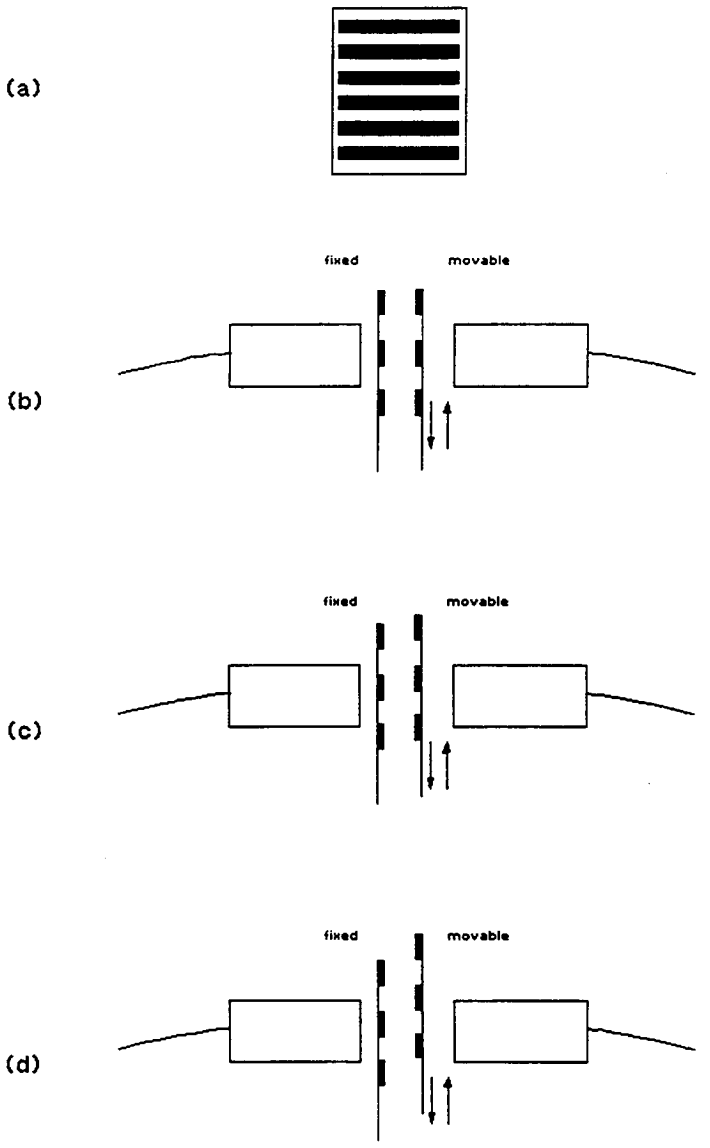

Fig. 2-6 (a) Illustration of sensitivity improvement, (a) gratings, (b) maximum, (c) partial, (d) no transmission.

3

Design and Principles of Operation of the Proposed Weigh-In-Motion Sensor

The proposed sensor consists of two main parts, the optoelectronics part and the mechanical part. The optoelectronics part includes light source, photodetector, GRIN lens, optical fiber, and associated electronic circuits. The mechanical part includes pneumatic tube, rubber pad, diaphragm, steel hoses, and air-bleed valves. Essential features of individual components are addressed.

Optoelectronics

Drive Circuit for Light Source

A LED is used as the light source. When forward biased, an LED generates light at a specific wavelength. The wavelength of the emitted light depends on the material composition of the active layer in the LED structure. The LED used in the developed sensor emits light at wavelength $\lambda = 850nm$. The output power increases almost linearly with the input current. For the LED used in the displacement sensor, a current of 100 mA is recommended. A simple drive circuit for the LED is shown in Fig. 3-1 [17]. Assuming a turn-on voltage V_γ for the LED, the current I_D flowing in the circuit is obtained from

$$I_D = \frac{V_o - V_\gamma}{R_1 + R_2}. \qquad (3.1)$$

The variable resistor R_2 is to allow for the adjustment of current. For $V_o = 15$ V, $V_\gamma = 0.7$ V, $R_1 = 100\ \Omega$, and R_2 varying from 0 to 100 Ω, the current varies in the range $71.5\text{ mA} < I_D < 143\text{ mA}$. An intermediate setting for R_2 provides a current $I_D = 100$ mA .

Detection Circuit

The light detector is a semiconductor photodiode which converts the light energy into an electrical signal. Here a PIN diode is used as a light detection element. The PIN diode is reversed biased in order to create a strong electric field to separate the released electrons and holes in the intrinsic region of the PIN diode. A simple bias circuit is shown in Fig. 3-2a. The maximum value of R_L of 0.85KΩ is chosen such that the rise time is not increased considerably. Based on the photodiode equivalent circuit shown in Fig. 3-2b, the rise time is obtained from [18]

$$t_r = 2.19 R_L C_d. \qquad (3.2)$$

The photodiode used in the sensor has the following specifications

$\lambda = 850\ nm, \quad \rho = 0.45\ A/W,$
$t_r = 10\ nsec, \quad C_d = 1.4\ pF,$
and $I_d = 2.0\ nA,$

where λ, ρ, I_d, t_r, and C_d are wavelength, responsivity, dark current, rise time, and detector's junction capacitance, respectively. Substituting for T_r and C_d, $R_L = 815\ \Omega$ is obtained.

Another quantity of interest is the minimum detectable power which is obtained as

$$\rho = \frac{I_d}{p} \text{ and, } p = \frac{I_d}{\rho} \qquad (3.3)$$

$$p = \frac{2nA}{0.45 \frac{A}{W}}$$

$$\cong 4.44\ nWatts.$$

The minimum detectable power is, in fact, a measure of the minimum measurable weight. The detector output signal is amplified using a two-stage amplifier. Fig. 3-2c illustrates the diagram of a single stage amplifier. The first stage provides a voltage gain of 50 and the second stage a voltage gain of 20. Thus, a total voltage gain of 1000 can be achieved.

Evaluation of Sensor Response

To evaluate the response of the displacement sensor, a setup such as that shown in Fig. 2-4 or 2-5 is used. A micropositioner is used to simulate the displacement of the blocking element. A power meter is used as detector. Experimental data accumulated for transmission-based displacement sensor are tabulated in Tables 1, 2, and 3. The data in Table 1 correspond to the sensor configuration shown in Fig. 2-5 and are plotted in Fig. 3-3, while the data presented in Tables 2 and 3 correspond to the sensor configuration in Fig. 2-4. In Table 2, columns 2 and 3 correspond to the experimental data with the cross sectional area of GRIN lens completely exposed, and the data with two small crescent portions of GRIN lens area are darkened in Fig. 3-4b to improve linearity, respectively. Variations of measured normalized transmitted power versus normalized displacement x/a are shown for both cases in Fig. 3-4a. It is observed that darkening of the two small crescent portions of the GRIN lens slightly improves the linearity of response, but, of course, at price

of lowering the maximum transmitted power.

Sensitivity Analysis

Using a linear approximation, the relationship between P_t/P_i and x/a can be expressed as

$$P_t = P_i(1 - 0.5\frac{x}{a}). \quad (3.4)$$

The output voltage of the detector circuit is proportional to P_t ; that is,

$$V_{out} = kP_t, \quad (3.5)$$

where k depends on the responsivity of the photodiode and the gain of the amplifier. Combining equations 3.4 and 3.5, yields

$$V_{out} = kP_i(1 - 0.5\frac{x}{a}). \quad (3.6)$$

Sensitivity is defined as

$$S = |\frac{\Delta V_{out}}{\Delta x}| = 0.5k\frac{P_i}{a}. \quad (3.7)$$

In equation 3.7, the GRIN lens radius, a, is fixed. Thus, to increase the sensitivity, the power emitted from the source or the gain of the amplifier stage may be increased. As mentioned earlier, the sensitivity may also be increased using a pair of gratings. To illustrate sensitivity improvement, setups of Figs. 2-4 and 2-5 are used with a grating having a period of about 1mm to detect displacements as small as 0.5mm. The experimental data are tabulated in Table 3 and plotted in Figs. 3-5 and 3-6, respectively. Because the data collected are many in number, only the data for first few cycles are given in Table 3. The variations of detected power in a displacement range of about 1mm, and the impact of using grating to improve sensitivity is highlighted in Fig. 3-7. It is evident that the use of gratings results in an increase in the slope of the response and thus, an increase in the sensitivity. Furthermore, by counting the number of fringes, one can readily determine the displacement accurately. For the present application, an adequate sensitivity can be achieved without the use of gratings.

Mechanical Components

Pneumatic Tube

The tube is an expandable hose with an inner diameter of 0.25 inches. It is housed in a rubber pad which serves as a mechanical support. The tube is connected at both ends to flexible but non-expandable stainless steel hoses, and is terminated to an air-bleed valve at each end. The longer end hose also transmits the fluid pressure to the diaphragm within the optical sensor assembly. The tube is filled with an incompressible fluid; water is used in laboratory experiments.

Rubber Pad

The pad is used mainly for mechanical support and to transmit evenly the applied load to the encased expandable tube. The material composition of the

manufactured pad is 1618.2 grams of resin, 4046 cc of softening agent, and 355.2 grams of curing agent. The hardness of the rubber pad plays a significant role in the operation of the sensor system. The harder the pad, the greater the amount of loads that can be applied. Mechanical properties of the pad also influence the response of the system both quantitatively and qualitatively. The influence of pad on the output voltage of the optical sensor, however, can be accommodated through calibration.

Diaphragm

The diaphragm is made of stainless steel and is placed between the optical displacement sensor and the flexible steel hose. The applied pressure causes the diaphragm to deflect. One side of the diaphragm is attached to a light blocking element, as that shown in Fig. 2-5. Thus, the diaphragm converts the pressure into displacement.

Steel Hoses and Air-Bleed Valves

Two steel hoses, one 6 feet long and another one foot long, are used. The function of the longer steel hose is to transmit the pressure, with minimal loss, from the load region to the location of the optical displacement sensor to which the diaphragm is attached. The shorter steel hose is to facilitate the removal of trapped air bubbles. Two air-bleed valves, one at each end of the pressure sensor assembly, are used to remove any trapped air in the system.

Table 1. Experimental data for a simple transmission-based pressure sensor.

Displacement (mm)	Voltage (V)	Displacement (mm)	Voltage (V)
0.000	10.0	0.525	3.8
0.025	10.0	0.550	3.6
0.050	9.8	0.575	3.4
0.075	9.5	0.600	3.2
0.100	8.5	0.625	2.9
0.125	8.0	0.650	2.7
0.150	7.5	0.675	2.5
0.175	7.1	0.700	2.3
0.200	6.7	0.725	2.1
0.225	6.2	0.750	1.9
0.250	6.0	0.775	1.7
0.275	5.7	0.800	1.6
0.300	5.5	0.825	1.4
0.325	5.3	0.850	1.2
0.350	5.1	0.875	1.1
0.375	4.9	0.900	0.9
0.400	4.7	0.925	0.7
0.425	4.5	0.950	0.4
0.450	4.3	0.975	0.3
0.475	4.1	1.000	0.1
0.500	4.0	-	-

Table 2. Experimental data for illustration of improving linearity.

Displacement (mm)	$P_t/P_i(1)$	$P_t/P_i(2)$
0.0	1.0	1.0
0.2	1.0	1.0
0.4	1.0	1.0
0.6	1.0	1.0
0.8	1.0	1.0
1.0	0.977	1.0
1.1	0.977	1.0
1.2	0.977	1.0
1.3	0.955	1.0
1.4	0.955	1.0
1.5	0.933	0.977
1.6	0.891	0.955
1.7	0.871	0.912
1.8	0.832	0.871
1.9	0.794	0.832
2.0	0.759	0.794
2.1	0.724	0.741
2.2	0.661	0.676
2.3	0.617	0.631
2.4	0.575	0.575
2.5	0.513	0.513
2.6	0.468	0.457
2.7	0.417	0.407
2.8	0.363	0.347
2.9	0.316	0.302
3.0	0.269	0.251
3.1	0.229	0.204
3.2	0.195	0.162
3.3	0.155	0.126
3.4	0.126	0.095
3.5	0.10	0.068
3.6	0.076	0.045
3.7	0.059	0.026
3.8	0.045	0.020
3.9	0.033	0.019
4.0	0.026	0.019
4.4	0.017	0.018
4.8	0.017	0.018
5.0	0.017	0.018

Table 3. Experimental data for illustration of sensitivity improvement.

Displacement (mm)	with GRIN lens Voltage (V)	without GRIN lens Voltage (V)
0.0	7.4	9.8
1.0	7.4	9.8
2.0	7.4	9.6
2.5	7.3	3.6
2.6	7.2	1.6
2.7	7.1	0.6
2.8	7.0	2.3
2.9	6.9	3.6
3.0	6.5	6.0
3.1	5.8	7.6
3.2	5.0	6.9
3.3	4.0	4.7
3.4	2.9	2.6
3.5	1.3	1.0
3.6	0.6	0.9
3.7	0.7	3.1
3.8	2.3	5.4
3.9	4.0	7.7
4.0	5.5	6.0
4.1	7.4	4.7
4.2	4.4	2.4
4.3	2.6	1.0
4.4	0.9	2.0
4.5	0.5	3.8
4.6	1.6	6.0
4.7	3.5	7.6
4.8	5.1	7.2
4.9	7.3	5.5
5.0	4.2	3.3
5.1	2.4	1.5
5.2	0.9	0.8
5.3	0.5	2.2
5.4	2.0	3.6
5.5	3.6	5.9
5.6	5.2	7.7
5.7	7.4	6.2
5.8	4.8	4.4
5.9	3.4	2.4
6.0	2.0	0.8

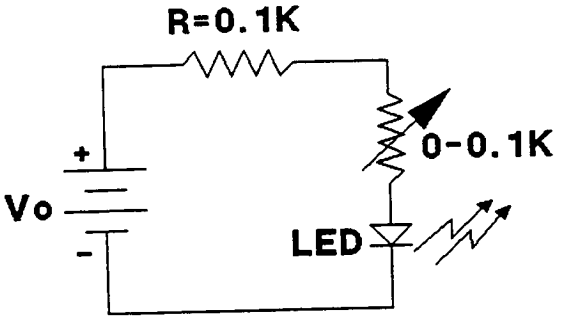

Fig. 3-1 Drive circuit for LED.

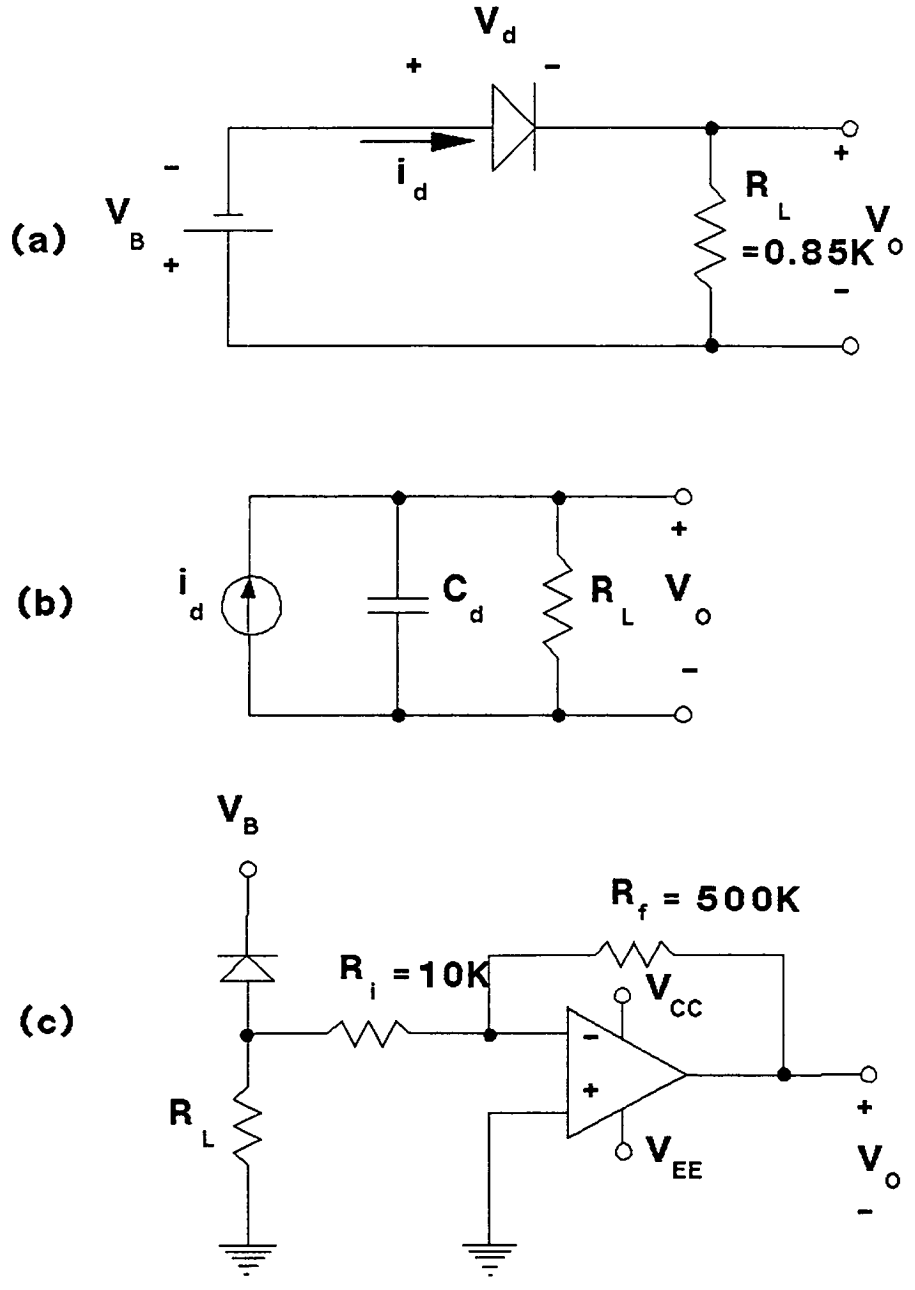

Fig. 3-2 (a) Bias circuit for photodiode, (b) equivalent circuit for photodiode, and (c) amplifier circuit.

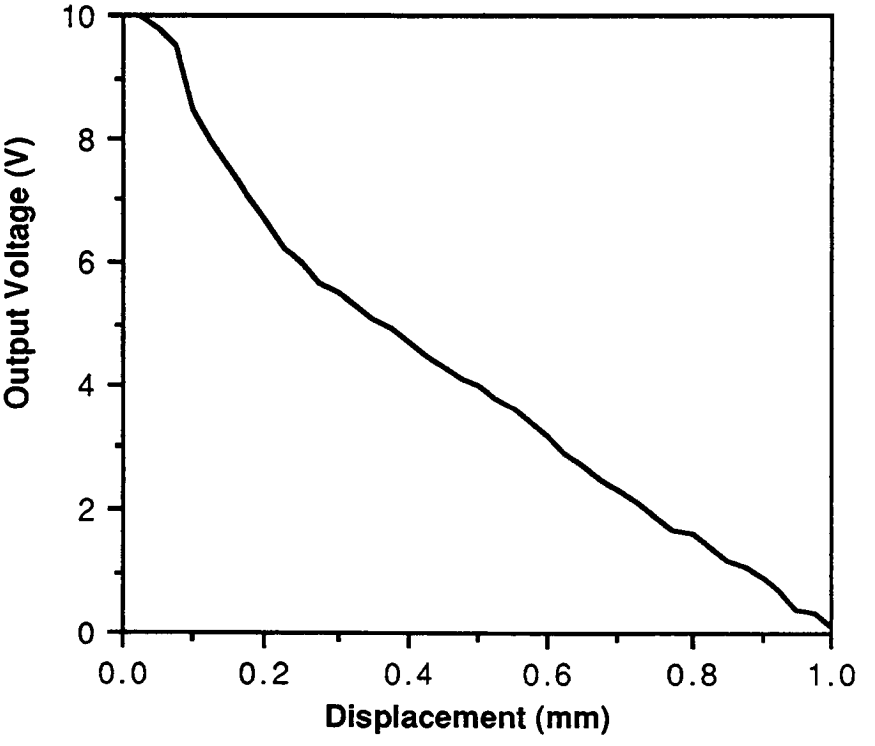

Fig. 3-3 Plot of data for a simple transmission-based pressure sensor.

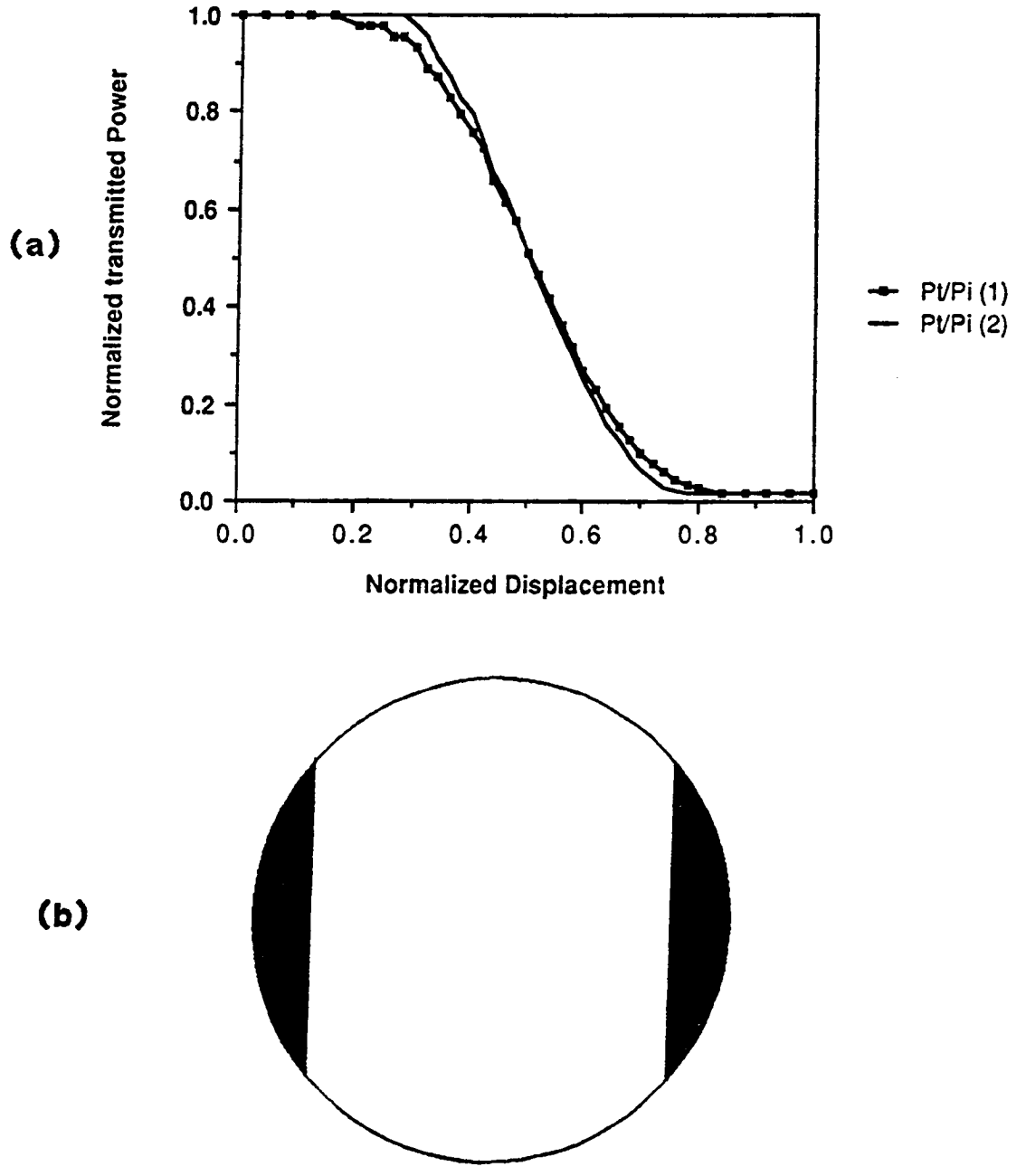

Fig. 3-4 (a) Variations of normalized transmitted power versus normalized displacement and (b) blackened areas improve the linearity of response.

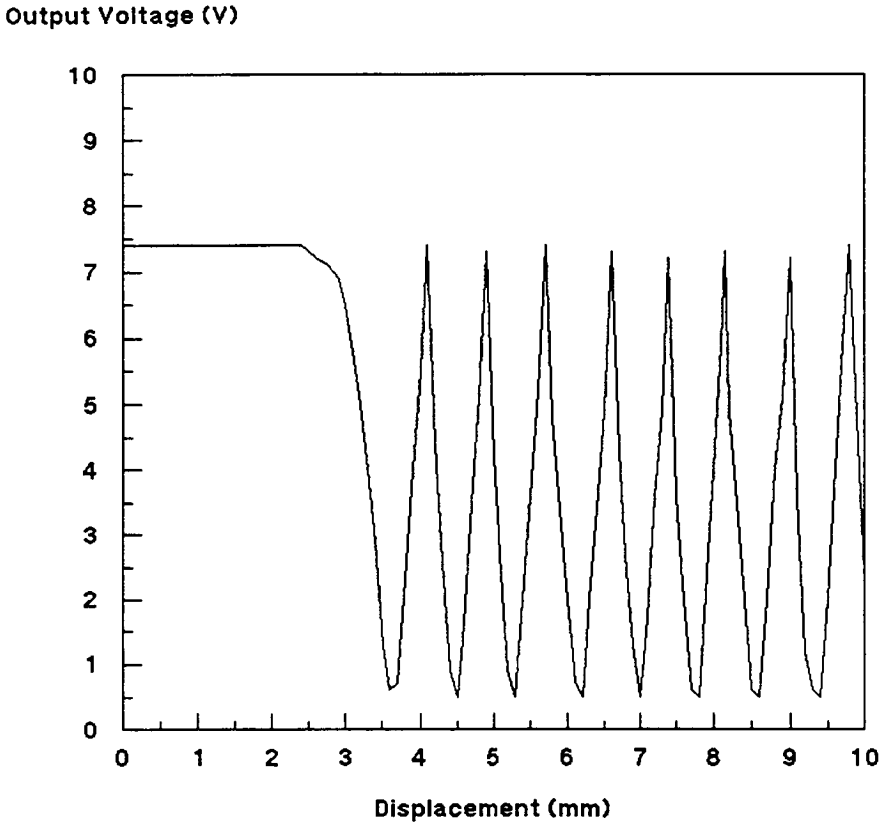

Fig. 3-5 Plot of experimental data for transmission-based pressure sensor with GRIN lens.

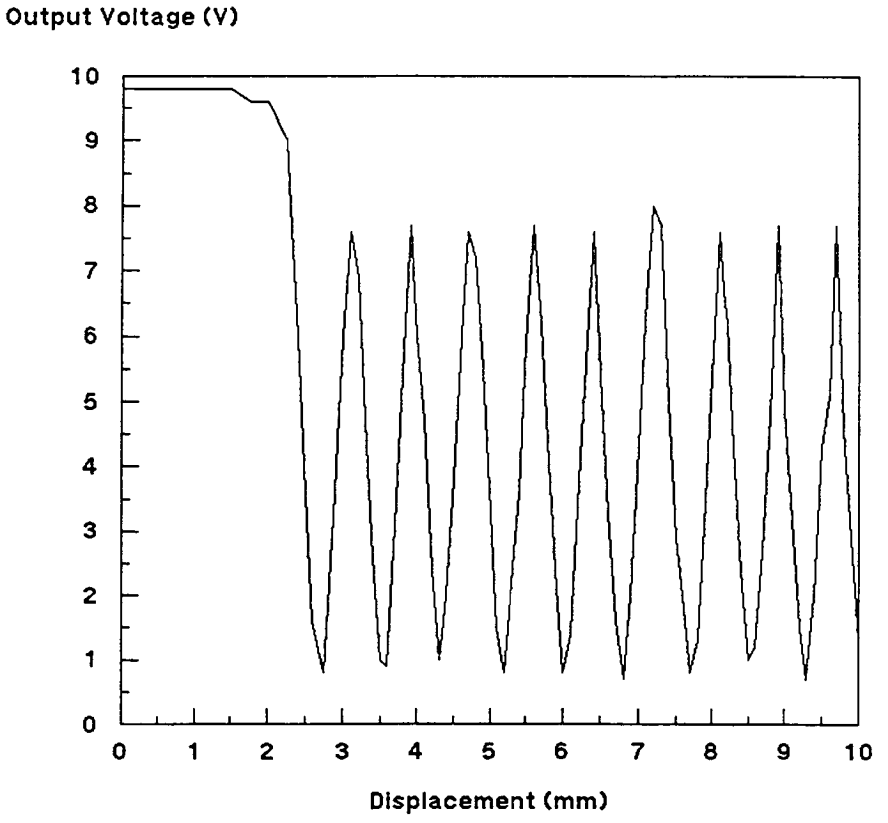

Fig. 3-6 Plot of experimental data for transmission-based pressure sensor without GRIN lens.

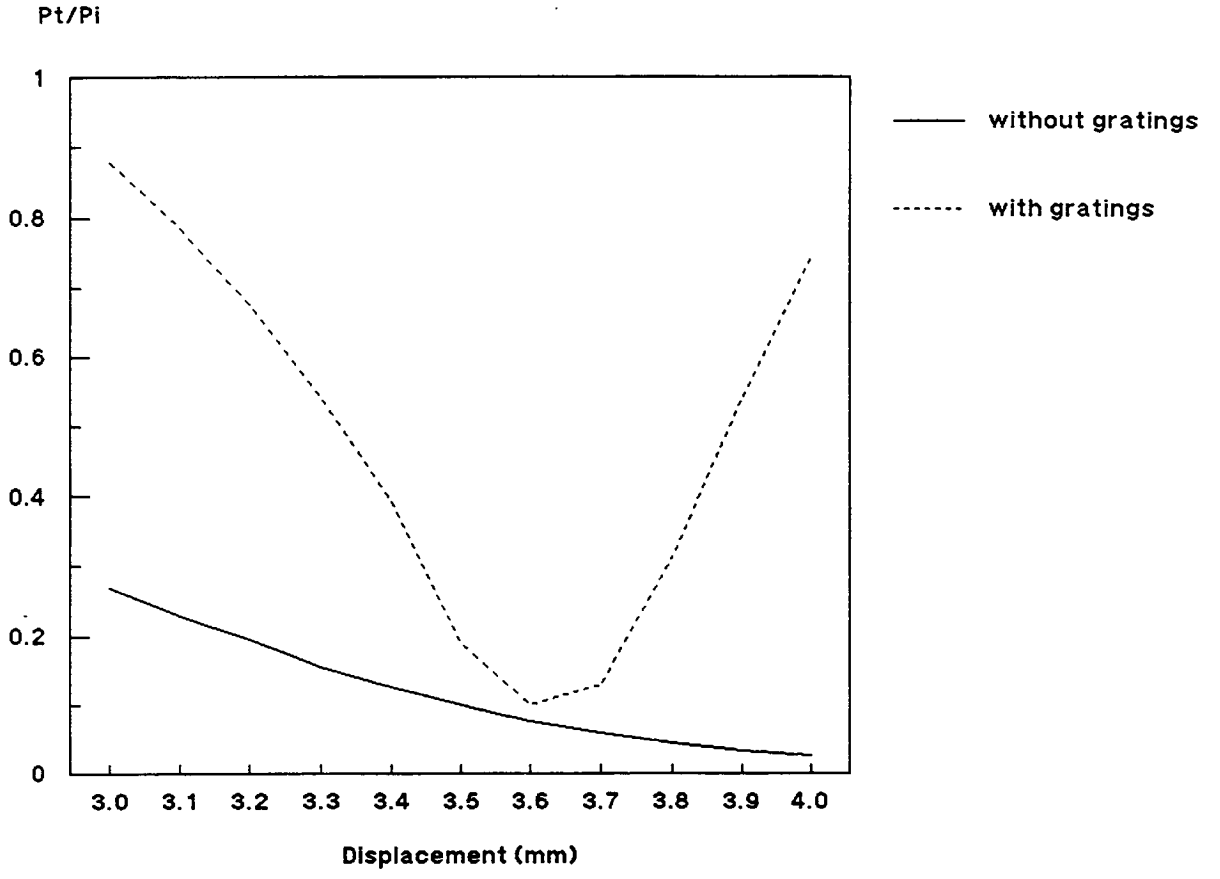

Fig. 3-7 Illustration of increased slope of response when gratings are implemented.

4

Laboratory Tests and Performance Evaluation of the Proposed Weigh-In-Motion Sensor

To evaluate the sensor performance under varying load frequencies, a series of experiments are performed using an MTS machine to simulate different vehicle weights and speeds. Statistical analyses of data are performed to assess the frequency dependence and the linearity of the sensor response.

Preparation for Laboratory Tests

Prior to laboratory tests, the sensor assembly needs to be packaged and filled with an incompressible fluid. Various components of the sensor system were carefully assembled to ensure that fluid would not leak out when pressure is applied. For convenience, water was used for laboratory tests, because it is incompressible and largely insensitive to minor temperature variations of the laboratory environment. The block diagram of the sensor assembly is shown in Fig. 4-1. Two metallic support plates each with an area of 72 in^2 were constructed to facilitate the application of load by the MTS machine. Two wooden columns also were made for supporting the steel hoses in order to dampen out undesired vibrations.

Experiments with the Sensor System

The rubber pad was mounted onto the stationary upper plate of the MTS machine. Load was applied from below through the metallic support plates. The optical displacement sensor was powered with a power supply providing an output voltage of 30 volts. Both the MTS load

signal and the output signal of the displacement sensor were monitored using a dual channel oscilloscope. The block diagram of the experimental setup is shown in Fig. 4-2.

A 20-Kip MTS machine was used and ten levels of load were applied. Each load was applied at different frequencies of 0.25, 0.5, 1, 2, 5, and 10 Hz. The applied loads were 1 Kip to 5.5 Kips in 0.5 Kip increments. Several cycles of a square wave were applied at each load-frequency combination (see Table 4). A square wave was used so that the sensor was loaded during half of each cycle. For example, for a load at 1 Hz frequency (1-second period), each cycle is 1 second long, and the sensor is loaded for 0.5 seconds in each cycle. The input and output signals were monitored simultaneously and photographed following each load application. The output signals were obtained for fifty eight load-frequency combinations summarized in Table 4. For 5 Kips and 5.5 Kips loads at 10 Hz, the pneumatic pad appeared to reach its maximum tolerance. Thus, to avoid permanent deformation of the pad, tests at these load-frequency combinations were not performed over a long enough duration and consistent readings for the output voltage were not obtained. The output waveforms were photographed for all cases, but, in order to limit the number of figures, only waveforms corresponding to 1 Kip, 2 Kips, and 4 Kips at frequencies of 0.25, 2, 5, and 10 Hz are presented here. Figs. 4-3 through 4-5 illustrate these waveforms. Each figure shows two waveforms; the upper waveform represents the sensor output signal, while the lower one corresponds to the MTS load signal.

Analysis and Discussion of Results

Examination of the output waveforms indicates that the initial application of the load induces a voltage which linearly follows the input voltage waveform. A ringing appears in the output waveform which increases with frequency of application, as the rubber pad is relieved of the applied compression. The ringing can be attributed to the oscillation of diaphragm, fluid wave interactions, and the mechanical response time-lag of the rubber pad. The system response is a function of the hardness of the rubber pad, which, in turn, is a function of the material used in fabricating the pad. The harder the rubber pad, the more sustained will be the oscillations and ringing effects. By properly selecting the incompressible fluid and choosing the right material composition for the pad, these problems can be largely alleviated. Unlike the piezoelectric cable where nonlinearities are evident in the low frequencies of applied loads (discussed in Chapter 5). For the optical sensor a linear behavior is more clearly demonstrated at lower frequencies as seen in Figs. 4-3a through 4-5a which correspond to 0.25 Hz frequency. At this frequency, the load waveform is nearly a square wave, and so is the output waveform. At higher frequencies, e.g. 10 Hz, the input waveforms are not clean square waves, but, unlike the piezoelectric case, the output signals exhibit peaks at instants

of application and removal of the load, just as in the case of low frequency loads. In general, however, the variation of the output signal with time for the high frequency loads is more pronounced, but the output waveform still follows the input waveform in a nearly piecewise linear fashion.

Overall, the optical sensor delivers a response much less dependent on the frequency of applied loads than does the piezoelectric cable sensor. Statistical analyses are performed to verify the above conclusions.

Fig. 4-6 compares variations of the half-cycle average output voltage versus load at six different frequencies of application. It is evident that for loads less than 5 Kips, the sensor response is highly linear as well as frequency independent. For loads higher than 5 Kips, the sensor response begins to exhibit nonlinearity, and, at a sufficiently high load, the expandable tube would buckle causing saturation of the output voltage. The behavior of the sensor response is largely influenced by the performance of the rubber pad and the expandable tube, and, to a less extent by the performance of the diaphragm. The rubber pad responds linearly only in a certain pressure range. Outside this range, the pad functions nonlinearly and may suffer permanent deformations. It is, thus, very important to design the pad such that it behaves linearly in response to the loads in the range of interest.

Fig. 4-7 is the best-fit regression line through the data. The regression results yield $y = -0.475 + 0.984x$, where y is the output signal in volts and x is the applied load in Kips. A coefficient of determination (R^2) equal to 99.5% is calculated which is an indication of high linearity of the sensor response. The t-values for the intercept and slope are -16.30 and 100.67, respectively, indicating that both the intercept and slope are significantly different from zero.

The dependency of the output signal on load frequency is statistically verified through two-sample t-tests with the results summarized in Table 5. The p-values resulted from 2-sample t-tests suggest that for a level of significance less than or equal to those shown in this table, the frequency dependence of the sensor from one frequency to the next is not significant. Of course, the accuracy of these results will increase several fold if the increments of applied load are decreased and the frequency is changed to smaller increments. Further examination of the data in Table 4 yields coefficient of variation values in a narrow range of 0 to 5.5% for the applied loads of 1 Kip through 5.5 Kips, thus signifying very little variations in output signals for a given load at various frequencies. Moreover, Figs. 4-6 and 4-7 do indicate that the sensor response exhibits a high degree of linearity, thereby a high accuracy in correlating the sensor response to the actual vehicle weight.

Table 4. Experimental data for the proposed WIM sensor.

	Average Output Voltage(V)						
Load(Kips)	0.25 Hz	0.5 Hz	1.0 Hz	2.0 Hz	5.0 Hz	10.0 Hz	Coeff. of Variation
1.0	0.6	0.6	0.6	0.6	0.6	0.6	0
1.5	1.0	1.0	1.0	1.0	1.0	1.0	0
2.0	1.5	1.5	1.5	1.45	1.5	1.5	1.4%
2.5	2.0	2.0	1.8	1.8	1.8	1.8	5.5%
3.0	2.5	2.5	2.4	2.4	2.4	2.4	2.1%
3.5	3.0	3.0	2.9	2.9	2.9	2.9	1.8%
4.0	3.5	3.5	3.5	3.5	3.5	3.5	0
4.5	4.1	4.0	4.0	4.0	4.0	4.0	1.0%
5.0	5.0	5.0	5.0	5.0	5.0	-	0
5.5	6.0	6.0	5.8	5.8	5.8	-	1.9%

Table 5. P-values for 2-sample t-test on experimental data for the proposed WIM sensor.

	0.5 Hz	1.0 Hz	2.0 Hz	5.0 Hz	10.0 Hz
0.25 Hz	0.99	0.92	0.91	0.92	0.92
0.5 Hz		0.94	0.93	0.94	0.94
1.0 Hz			0.99	1.0	1.0
2.5 Hz				0.99	0.99
5.0 Hz					1.0

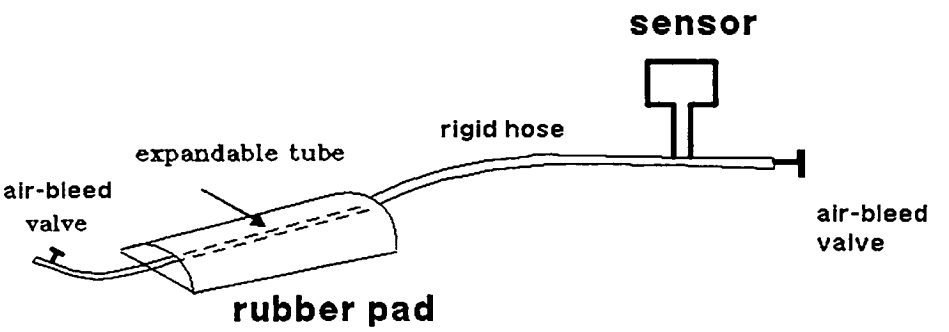

Fig. 4-1 Block diagram of pressure sensor assembly.

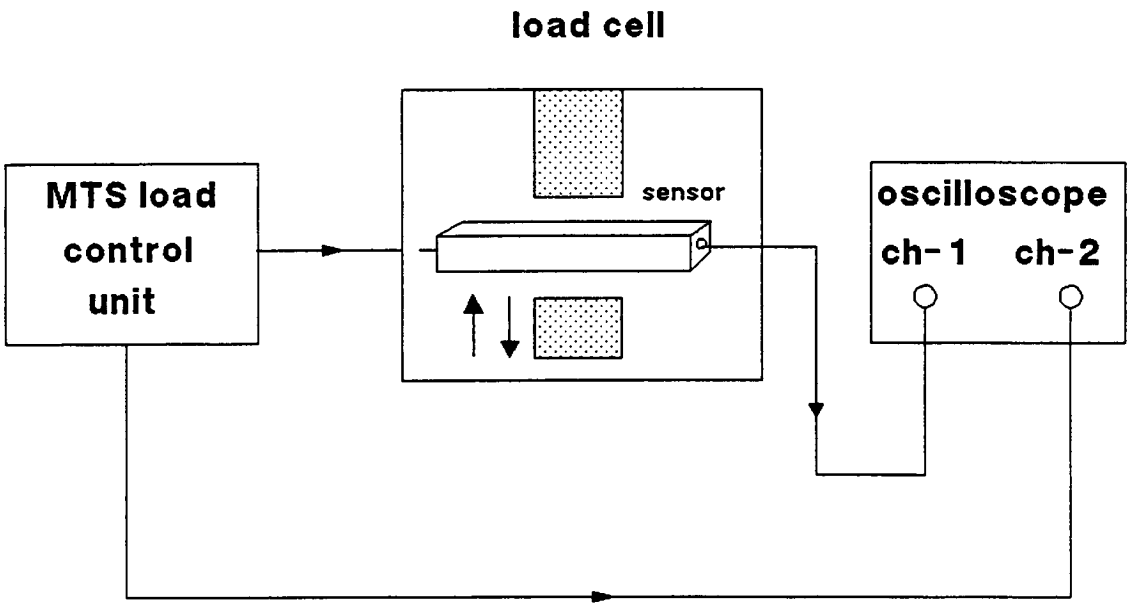

Fig. 4-2 Block diagram of the experimental set up for the pressure sensor.

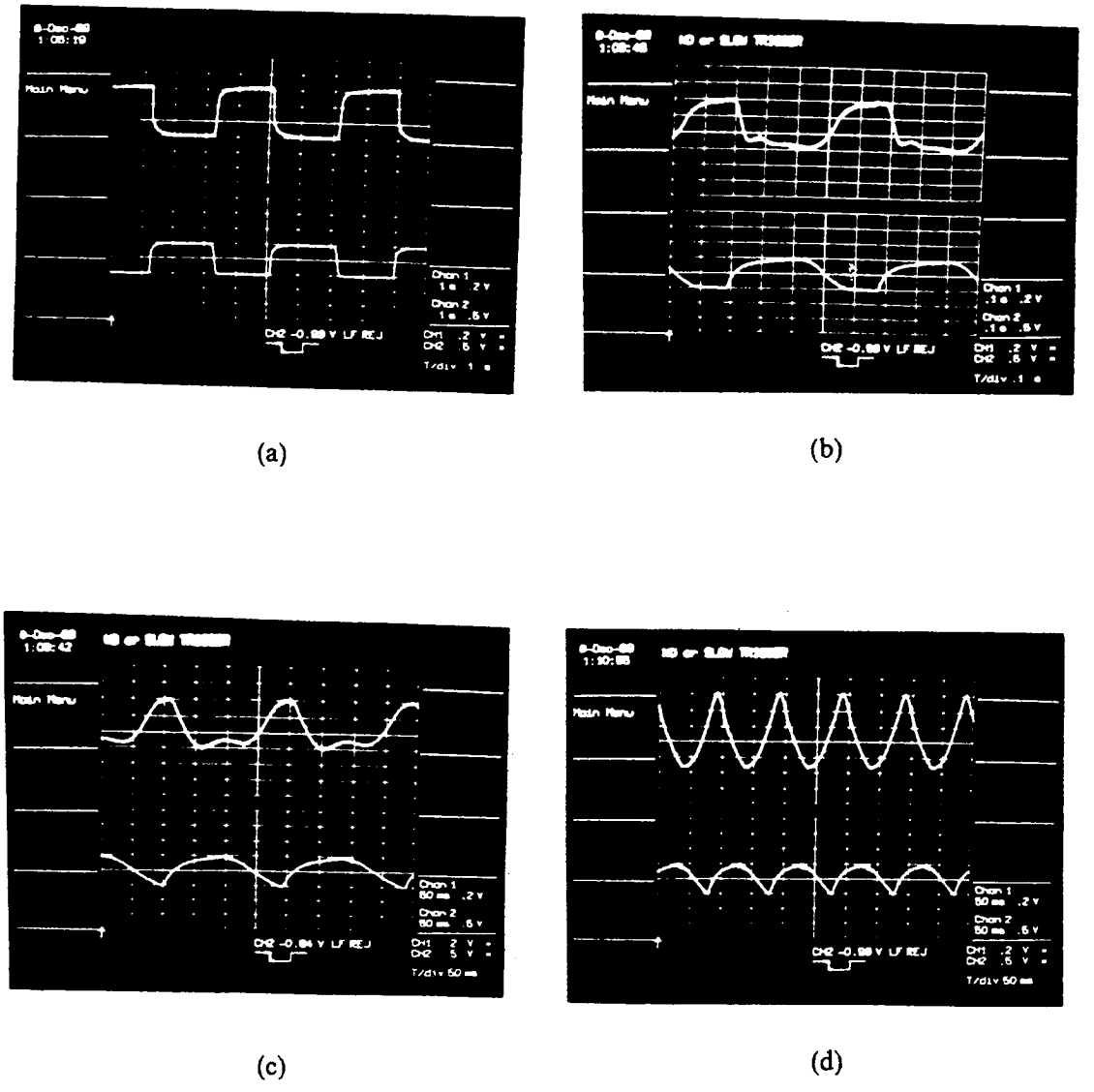

Fig. 4-3 Response of the sensor for 1 Kip load at frequency (a) 0.25 Hz, (b) 2 Hz, (c) 5 Hz, and (d) 10 Hz.

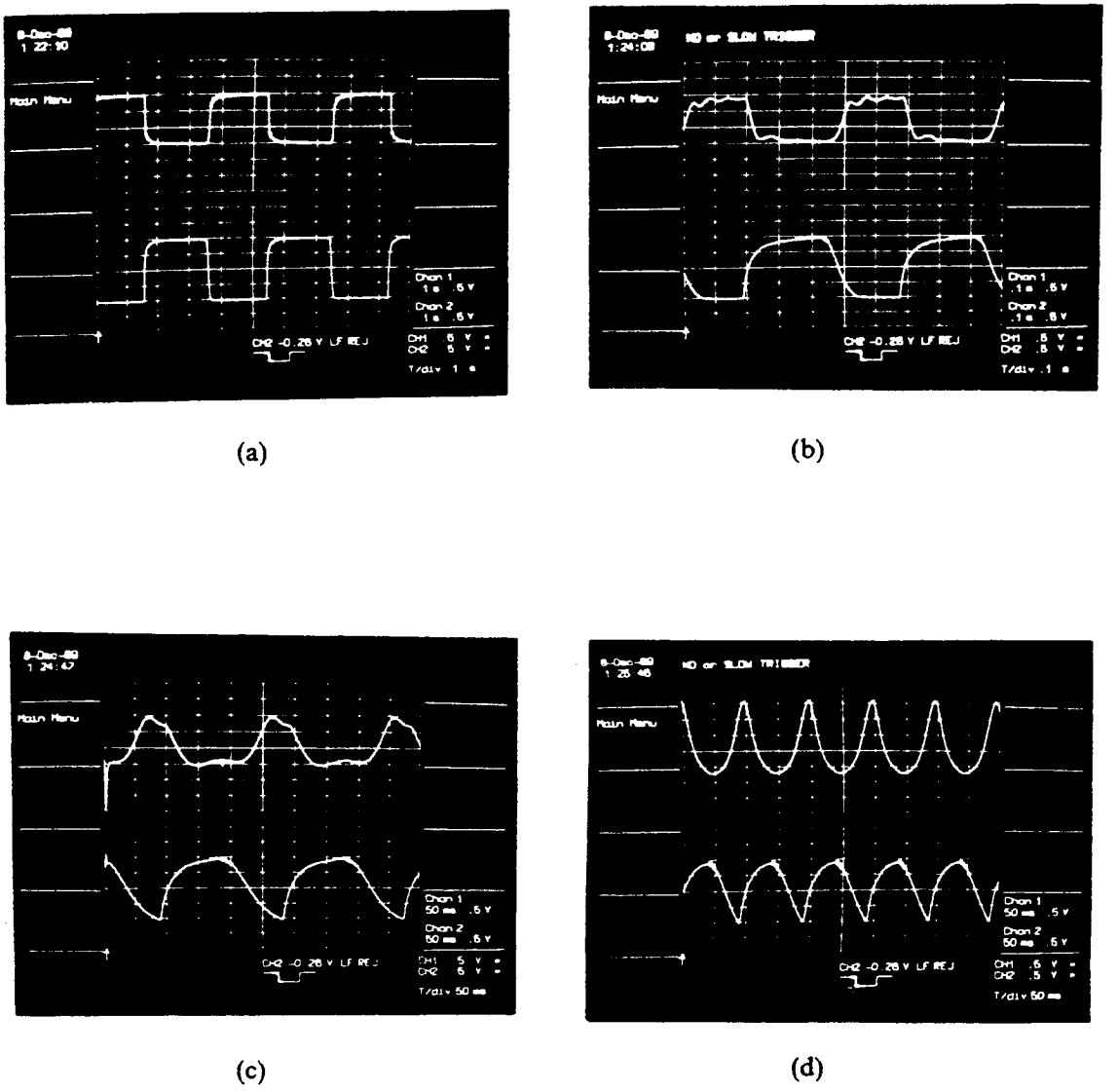

(a) (b)

(c) (d)

Fig. 4-4 Response of the sensor for 2 Kips load at frequency (a) 0.25 Hz, (b) 2 Hz, (c) 5 Hz, and (d) 10 Hz.

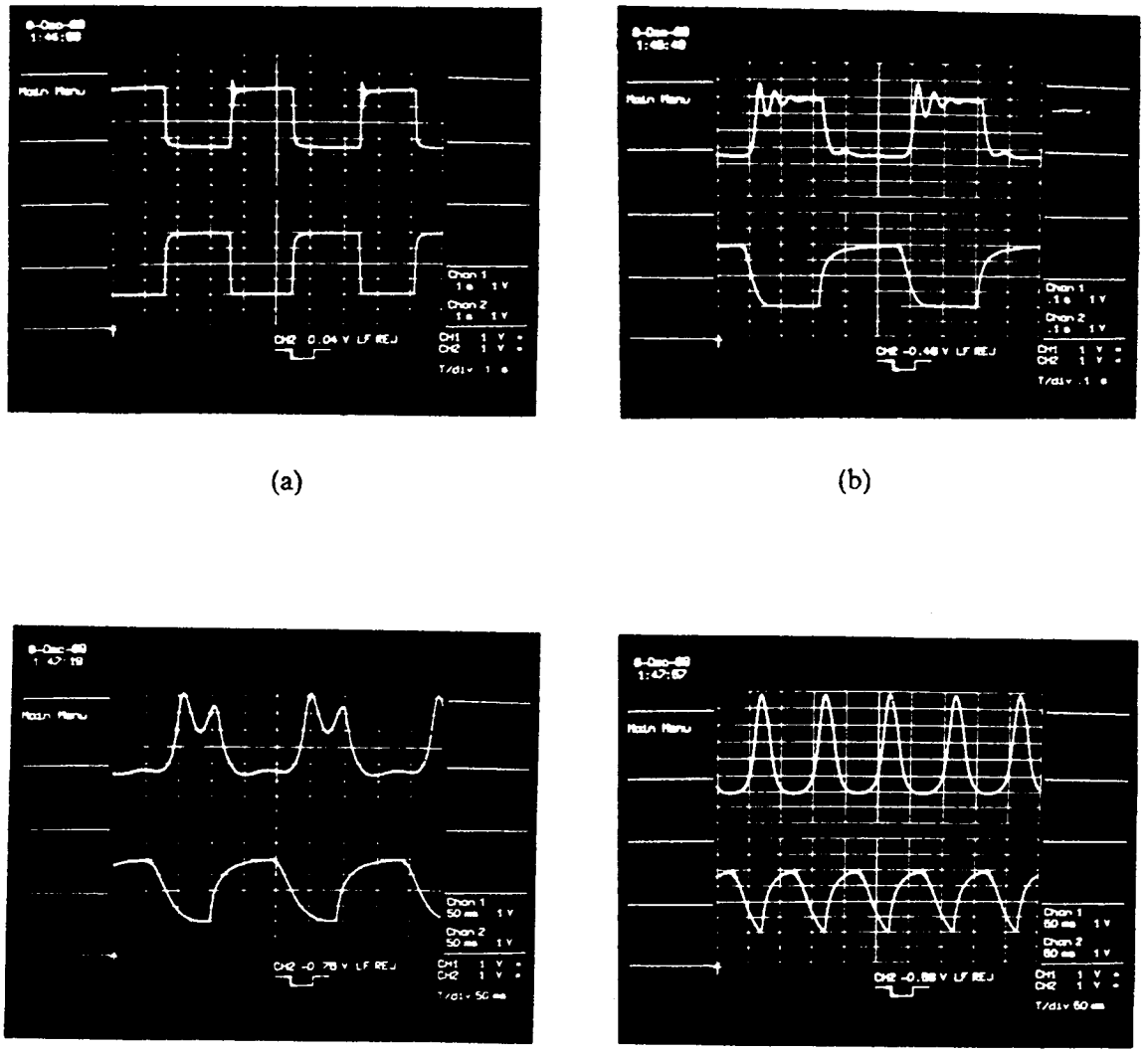

Fig. 4-5 Response of the sensor for 4 Kips load at frequency (a) 0.25 Hz, (b) 2 Hz, (c) 5 Hz, and (d) 10 Hz.

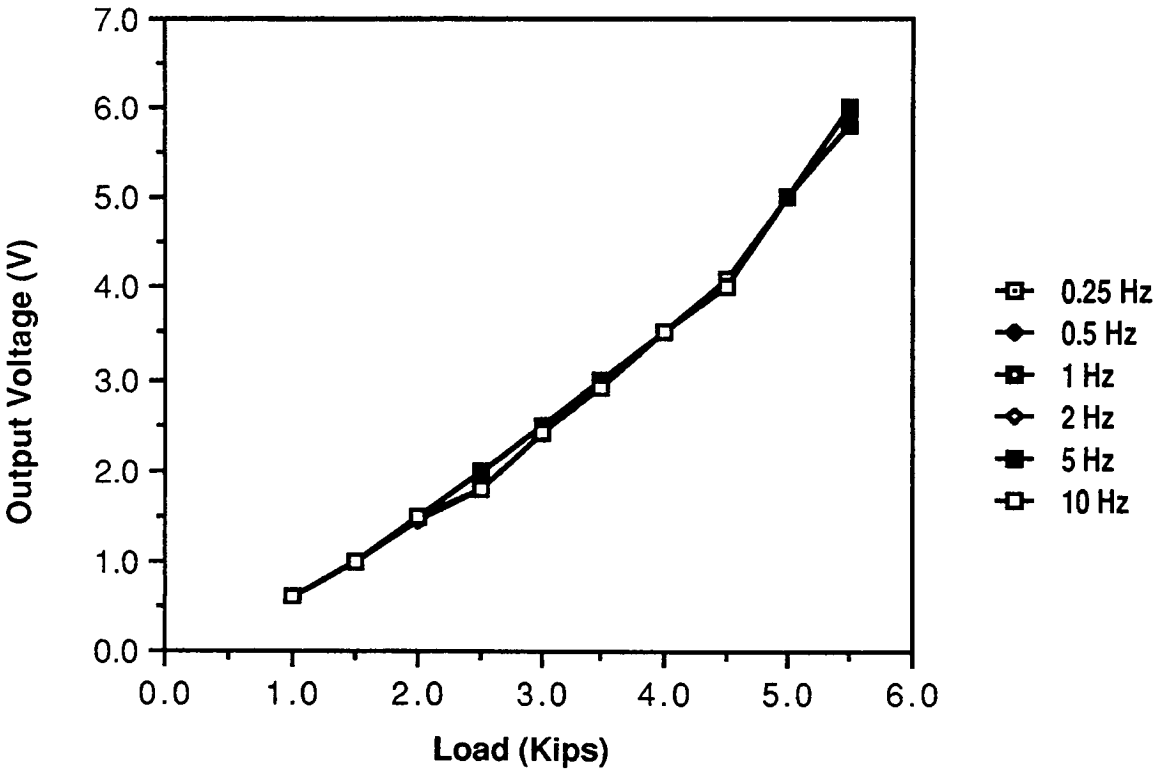

Fig. 4-6 Variations of the sensor output voltage with load at different frequencies.

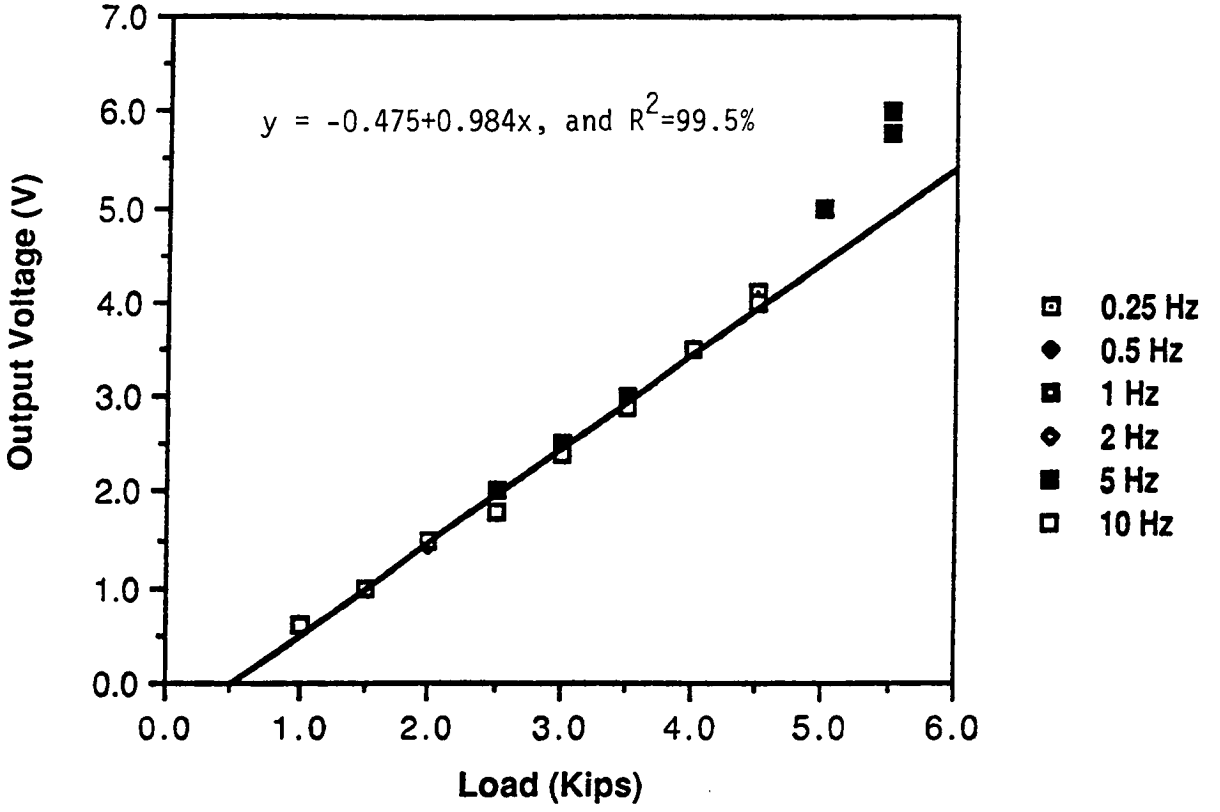

Fig. 4-7 Linear regression of the sensor data for varying frequencies of applied load.

5

Tests on Piezoelectric Sensor and Comparison with Proposed Weigh-In-Motion Sensor

The principle of operation of piezoelectric cable is briefly described. To compare the performance of piezoelectric cable under varying load magnitudes and frequencies with that of the proposed sensor, a series of experiments are carried out. The experimental setup is similar to that used for the optical sensor shown in Fig. 4-2.

Principle of Operation

A piezoelectric cable is essentially a coaxial cable, in which the region between the inner and outer conductors is filled with a piezoelectric material in the form of a compressed powder. The piezoelectric material acts as a dielectric for the coaxial cable. The material is poled by a radial electric field generated between the inner and outer conductors, thus allowing a piezoelectric response to radial stress [19]. Piezoelectricity is a property of some materials that manifests itself by the generation of electrical charges of opposite polarity when they are subjected to a mechanical stress. It arises because of an interaction between Coulomb forces and the elastic restoring forces [20]. The amount of charge induced depends upon the change of the applied pressure. In other words, the output voltage of a piezoelectric cable, which is proportional to the charge induced, depends upon the time derivative of the pressure and is not proportional to the pressure itself. Thus, a constant pressure gives rise to an output voltage which decreases with time.

Laboratory Experiments

The piezoelectric sensor used consists of a piezoelectric cable embedded in epoxied resin and housed in an aluminum frame of 20x20 *mm* cross section and is about 3.5 meters long. The sensor was mounted onto the stationary upper plate of an MTS machine. The piezoelectric cable was firmly supported by six wooden columns along its length, in order to dampen undesired vibrations. Load was applied from below through a specially prepared metallic support plate of about 10 in^2.

A 20-Kip MTS machine was used and five levels of load were applied (1 to 5 Kips in 1-Kip increments). Each load was applied at different frequencies of 0.25, 0.5, 1, 2, 5, and 10 Hz. Table 6 summarizes all load-frequency combinations. Several cycles of a square wave were applied at each load-frequency combination (see Table 6). A square wave was used so that the sensor was loaded during half of each cycle. The MTS was interfaced to an oscilloscope. The input and output signals were monitored simultaneously and photographed following each load application.

Traffic Conditions Simulated

The loading frequencies described above could represent a variety of combinations of speeds, axle spacings, and vehicle headways. For example, at 70 mph square waves of 0.25, 0.5, 1, 2, 5, and 10 Hz approximately correspond to spacings of 200′, 100′, 50′, 25′, 10′, and 5′, respectively. The large spacings corresponding to the lower frequencies of 0.25, 0.5, and 1 Hz generally represent vehicle headways, rather than axle spacing for most highway speeds. On the other hand, the upper frequencies of 2, 5, and 10 Hz are representative of typical truck axle spacings.

Fig. 5-1 shows the typical truck types on U.S. highways as documented by FHWA [21]. As an example, a typical 3S2 semi-trailer truck (Fig. 5-1) may have axle spacing of 10′, 5′, 25′, and 5′ between axles 1-2, 2-3, 3-4, and 4-5, from front to rear, respectively. At 70 mph, these axle spacings correspond to frequencies of 2, 5, and 10 Hz, respectively. A second example may be a 3S2-2 truck (Fig. 5-1) with axle spacings of 10′, 5′, 20′, 5′, 10′, and 25′ corresponding to respective frequencies of 5, 10, 2.5, 10, 5, and 2 Hz at 70 mph.

The magnitude of the loads applied ranged from 1 Kip to 5.5 Kips in the experiments for the two sensor types. The nominal loading plates were 72 in^2 and 10 in^2 for the fiber-optic and piezo sensors, respectively. Therefore, pressures ranging between approximately 14 psi (1 Kip, 72 in^2) and about 500 psi (5 Kips, 10 in^2) have been applied. This range of applied pressure is wide enough to incorporate the typical maximum truck tire pressure of about 100 psi.

Performance Under Varying Load Frequencies

Sensitivity to the frequency of the load applied is an aspect of the accuracy of the piezoelecric sensor particularly not addressed in the past. The output signal of the piezoelectric cable was obtained for each load-frequency combination. The output waveforms were photographed for all cases, but, in order to limit the number of figures, only waveforms corresponding to 0.25, 2, 5, and 10 Hz frequencies are presented here. Figs. 5-2 through 5-4 illustrate these waveforms for loads 1, 2, and 4 Kips, respectively. Each figure shows two waveforms. The upper waveform represents the piezoelectric cable output signal, while the lower one corresponds to the MTS load signal, which, hereafter, is referred to as the input signal.

An examination of the output waveforms indicates that the initial application of the load induces a voltage which rises rapidly from zero to a maximum value, then decreases in an exponential manner. After the load is removed, the output voltage undergoes another change reaching a negative peak which also decreases exponentially with time. It is, thus, evident that the response of the piezoelectric cable depends upon the time derivative of the applied load, i.e., df/dt. This behavior is more clearly demonstrated at lower frequencies, as seen in Figs. 5-2a through 5-4a, which correspond to 0.25 Hz frequency. At this frequency, the load waveform is nearly a square wave. At higher frequencies, the input waveforms are not clean square waves, but the output signals exhibit peaks at instants of application and removal of the load, as in the case of low frequency loads. In general, however, variations of the output signal with time for the high frequency loads is more complex, exhibiting an oscillatory behavior during the decay period. These oscillations may be attributed to residual vibrations of the cable at higher load frequencies. This difference in decay time of the induced voltage at low versus high frequencies could be an additional source of error in piezoelectric WIM systems.

Fig. 5-5 is a plot of the output voltage versus the load applied. Fig. 5-6 is the best-fit regression line through the data points, namely $y = -5.08 + 12.6x$, where y is the output signal (mV) and x is the applied load (Kips). The coefficient of determination (R^2) is 82.9% indicating a fairly linear relation between the applied load and the output signal. More importantly, the t-values for the intercept and slope are -1.45 and 11.91, respectively, with 28 degrees of freedom. These values correspond to levels of significance (p-values) of 0.158 and 0.000, respectively. It can, therefore, be concluded that, while slope is effectively zero the p-values suggest that the intercept is different from zero. Fig. 5-5 compares variations of the peak output voltage versus load at six different frequencies. It appears that the output signal is not independent of the applied frequency. For example, a 4-Kip load applied at a 10 Hz frequency generates the same voltage as a 3-Kip load at 0.25 Hz frequency. This simply implies that two

vehicles with different axial loads and speeds result in the same output response. Moreover, the cable response is not piecewise linear for loads greater than 3 Kips. This nonlinearity becomes more significant at higher frequencies. It must be noted that in Fig. 5-5, a decline in voltage is experienced upon the application of a 4-Kip load at frequencies under 10 Hz. This decline is due to unexpected failure of the steel support structure holding the piezoelectric cable during testing and not an inherent characteristic of the piezoelectric cable.

The dependency of the output signals on load frequency is statistically verified through two-sample t-tests the results of which are shown in Table 7. The output signal under each load frequency is tested against any other frequency for statistical significance of differences. The corresponding p-values are tabulated in Table 7, showing, for example, that the output signals at 2 Hz are different from those at 0.5 Hz at 86% level of significance or higher. Of course, the higher the p-values, the less significant the observed differences will be. In this regard, the matrix entries in Table 7 must be compared to the respective matrix entries for the fiber-optics WIM sensor results presented in Chapter 4. Further evidence of the output sensitivity to load frequency is obtained through examining the coefficient of variation of the output signals for each level of loading. Using the data in Table 6, coefficients of variation in the range of 8.4% to 33.5% are obtained for the loads of 1 to 5 Kips. While the variation is smallest for 2-Kips load (8.4%), in all other cases, the values are over 10% indicating relatively much larger errors due to frequency as compared to the fiber-optic sensor.

In summary, the piezoelectric sensor response over a wide range of applied loads displays rather large seemingly random errors with frequency of the applied load. These would make the correlation of the cable response to the axle weight of the vehicle a difficult task, as the voltage signal received for equally loaded axles would be different depending on the vehicle speed and axle configuration.

Comparison with Optical Sensor

In terms of the shape of the output signal, the piezoelectric sensor generated exponentially decaying output waveforms for square wave inputs. The optical sensor, on the other hand, provided square wave outputs for square wave inputs. In other words, the optical-sensor was reporting a constant voltage reading as long as the MTS loading cell was in contact with the sensor. On the contrary, the piezoelectric sensor output signal would peak to a maximum value proportional to the magnitude of the applied load but would drop back to zero regardless of if, or when, the load was removed. In processing the WIM sensor output signals, the area underneath the output signal wave is a desirable piece of information in determining the axle weights. Therefore, square wave output signals of the fiber-optic sensor offer a significant advantage over the exponen-

tially decaying output waves of the piezoelectric sensor.

Another advantage of the fiber-optic WIM sensor over its piezoelectric counterpart is in output signal variation with load frequency. The data indicate that the signal outputs vary considerably less with load frequency in the case of optical-sensor. The waveforms generated clearly established that the response of fiber-optic sensor is less frequency dependent. This indicates that the speed and axle spacing of vehicles could be a significant source of error in the piezoelectric WIM sensor, but not in the fiber-optic case.

The proposed fiber-optic sensor could offer considerably greater accuracy over the piezoelectric sensors. Both the output waveform and the lack of strong frequency dependence in the fiber-optic case greatly contribute to its accuracy. In addition, the fiber-optic signal is not susceptible to EMI. Furthermore, unlike the piezoelectric case, the electronic components in the optical sensor are not in direct contact with the wheel, thus they do not undergo permanent deformation and their bending characteristics are not altered. Finally, the optical sensors can be made temperature insensitive. The bending characteristics of the piezoelectric sensors, however, are shown to change at extreme temperatures experienced in the roadway environment.

The optical sensors could also offer a considerably lower life-cycle cost. They are portable and are installed over the pavement crown surface. As such they can be installed rapidly and with minimal traffic interruption, especially since there is no need to dig the pavement and embed the sensor, or affix it to the surface. The electronic components of the optical sensor are cheaper and readily available since they are mass produced for variety of other applications in the fiber-optics and communications fields. The electronic sensor components, which comprise a major fraction of the total sensor cost (over 60%), cost under $600 per sensor unit at the time of this writing. Furthermore, the electronic sensor components are installed on the side of the road and would never be in contact with the traffic, thus lasting longer. The above-mentioned attributes contribute to a lower life cycle cost of the optical sensor, as compared to other conventional WIM sensors in use today.

Table 6. Experimental data for piezoelectric sensor.

	Induced peak voltage(mV)						
Load(Kips)	0.25 Hz	0.5 Hz	1.0 Hz	2.0 Hz	5.0 Hz	10.0 Hz	Coeff. of Variation
1.0	4.0	5.0	5.0	3.0	5.0	8.0	33.5%
2.0	19.0	20.0	20.0	20.0	20.0	16.0	8.4%
3.0	40.0	25.0	33.0	45.0	36.0	30.0	20.5%
4.0	60.0	58.0	57.0	52.0	59.0	40.0	13.9%
5.0	52.0	48.0	41.0	48.0	46.0	68.0	18.4%

Table 7. P-values for 2-sample t-test on piezoelectric sensor experimental data.

	0.5 Hz	1.0 Hz	2.0 Hz	5.0 Hz	10.0 Hz
0.25 Hz	0.80	0.79	0.92	0.90	0.87
0.5 Hz		1.0	0.86	0.89	0.94
1.0 Hz			0.86	0.88	0.93
2.0 Hz				0.98	0.93
5.0 Hz					0.96

SINGLE-UNIT TRUCKS -

COMBINATION TRUCKS -

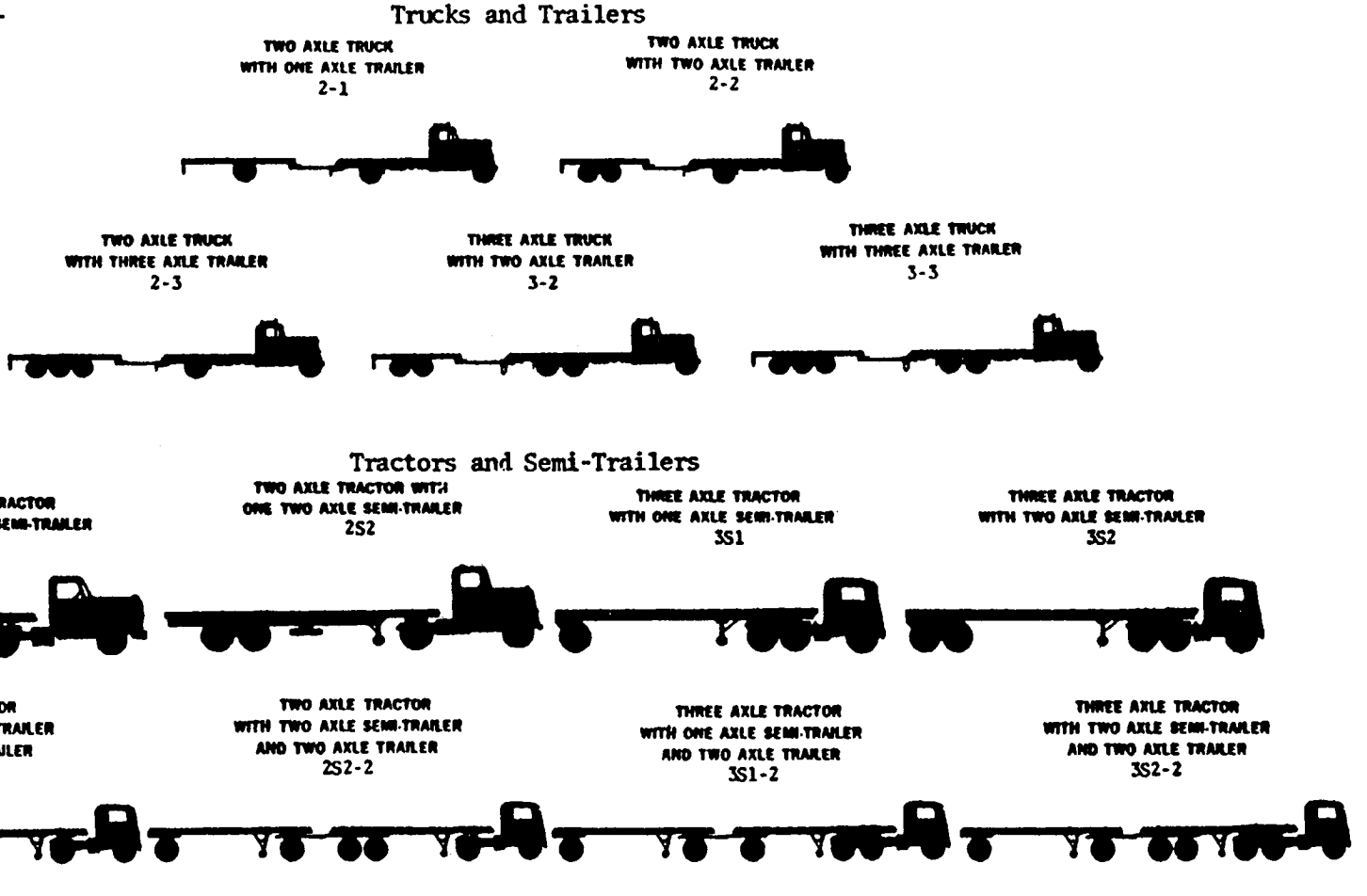

Fig. 5-1 Typical truck types [21].

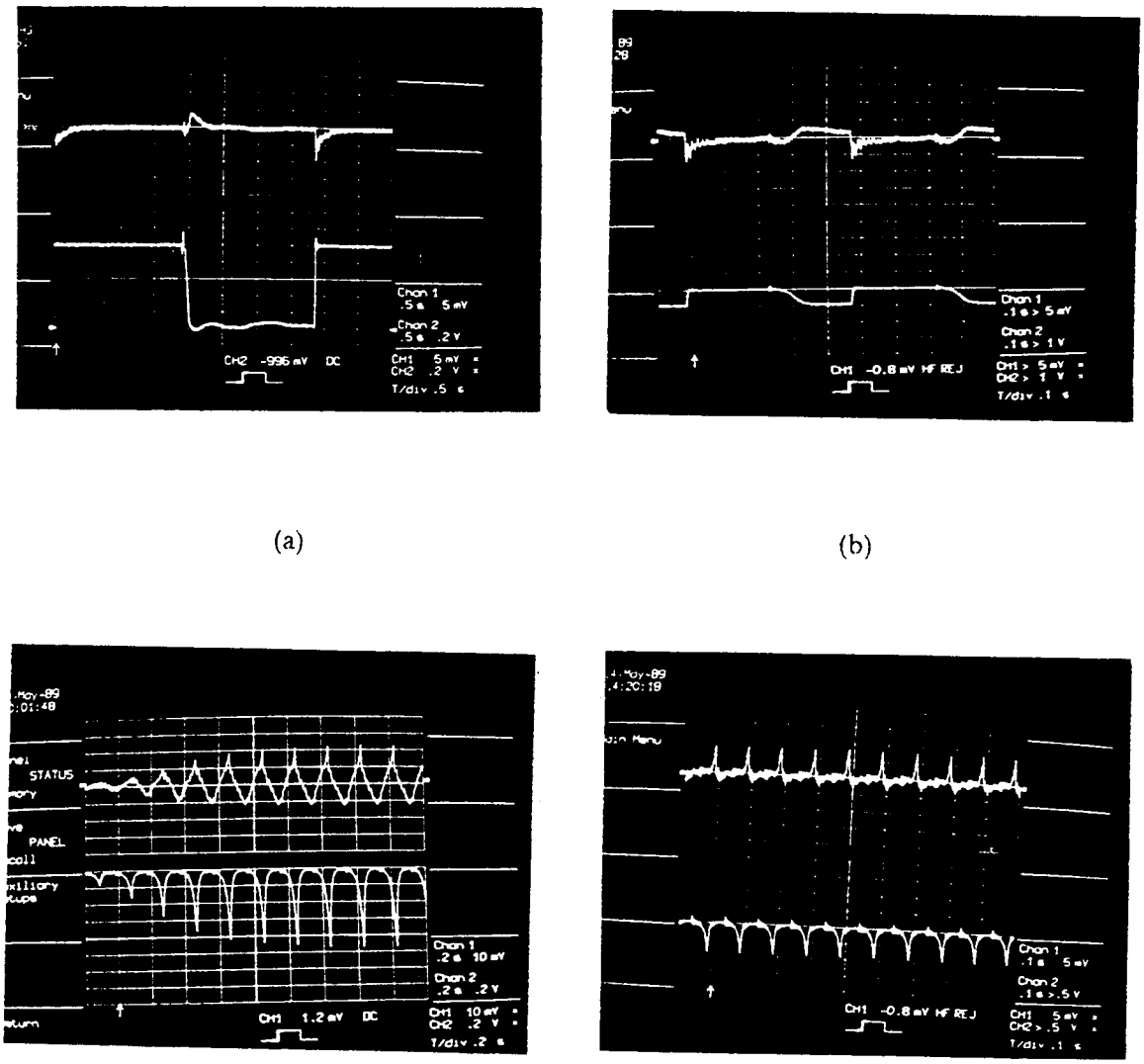

(a) (b)

(c) (d)

Fig. 5-2 Response of piezoelectric sensor for 1 Kip load at frequency (a) 0.25 Hz, (b) 2 Hz, (c) 5 Hz, and (d) 10 Hz.

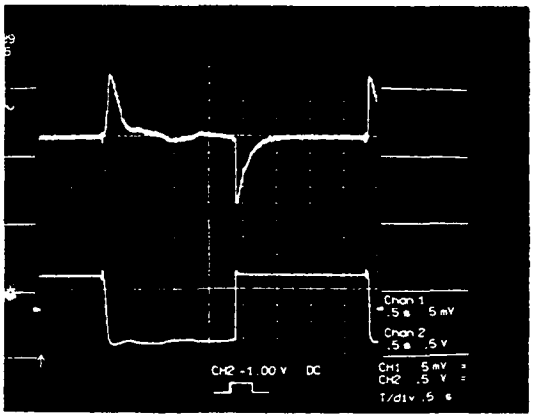

(a)

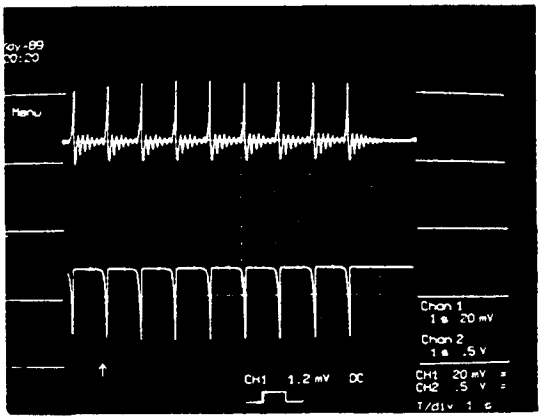

(b)

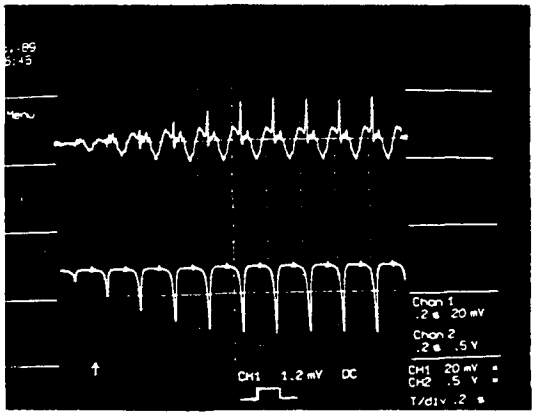

(c)

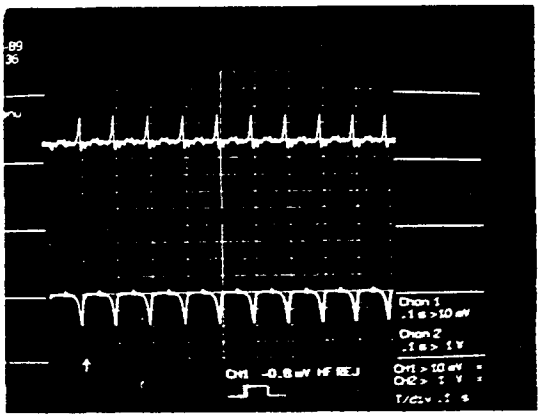

(d)

Fig. 5-3 Response of piezoelectric sensor for 2 Kips load at frequency (a) 0.25 Hz, (b) 1 Hz, (c) 5 Hz, and (d) 10 Hz.

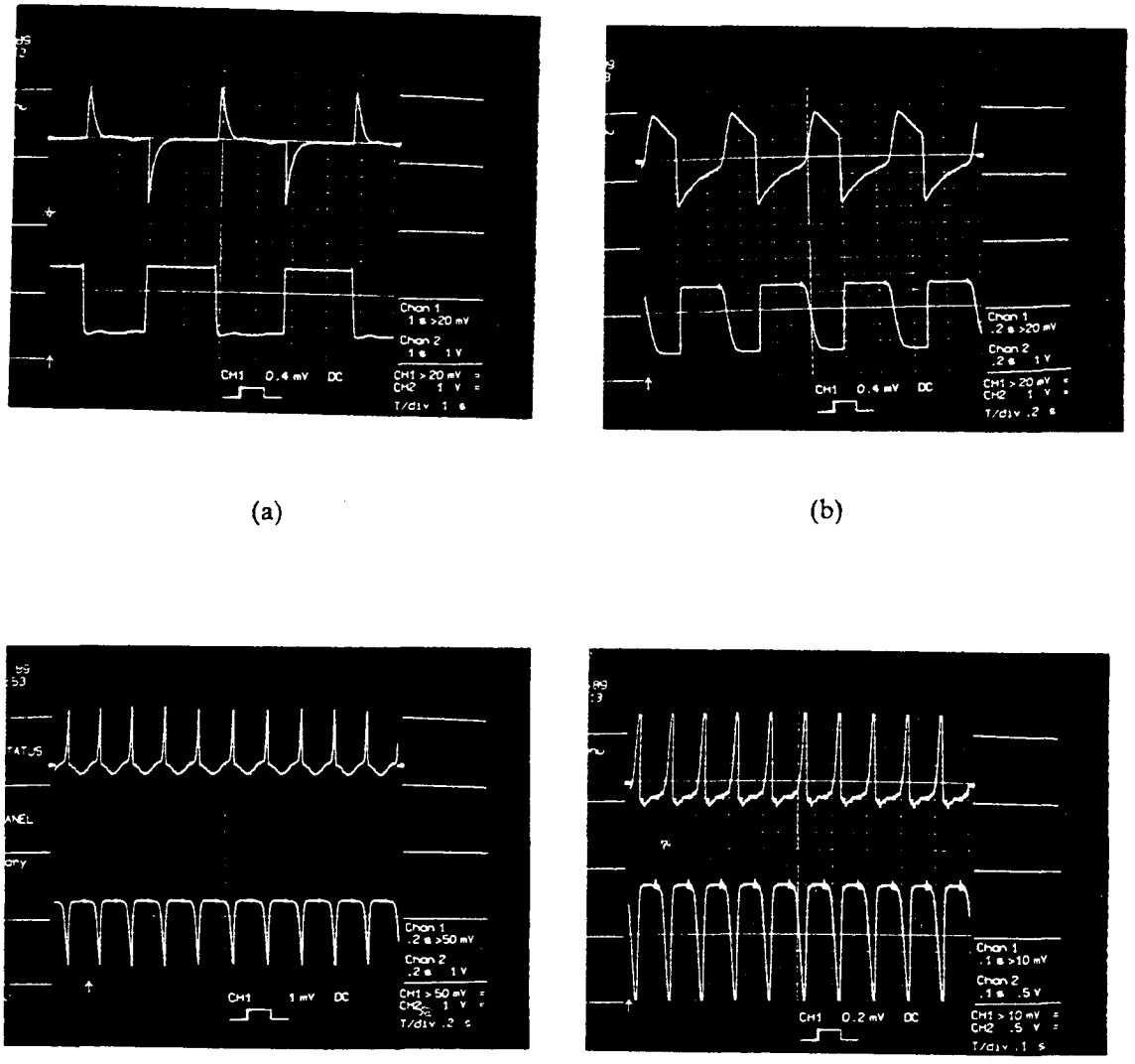

Fig. 5-4 Response of piezoelectric sensor for 4 Kips load at frequency (a) 0.25 Hz, (b) 2 Hz, (c) 5 Hz, and (d) 10 Hz.

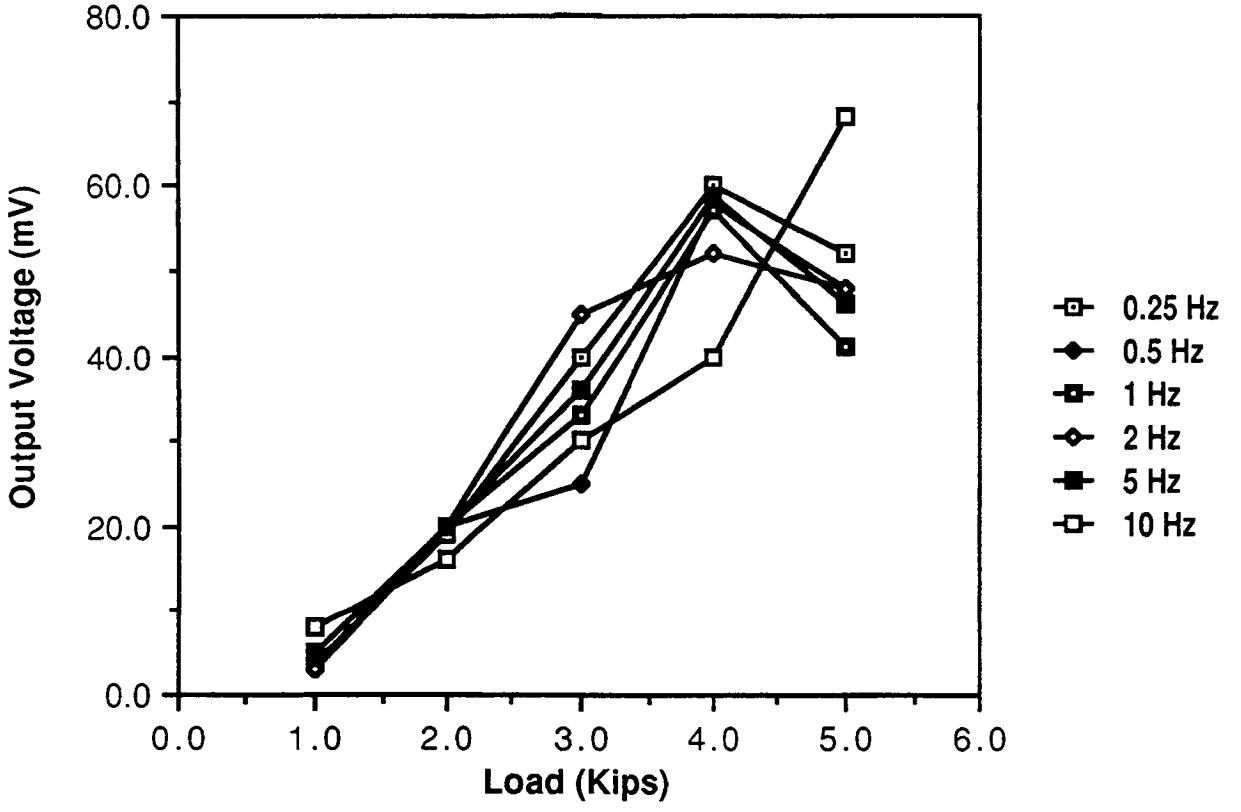

Fig. 5-5 Variation of piezoelectric cable output voltage versus load at different frequencies.

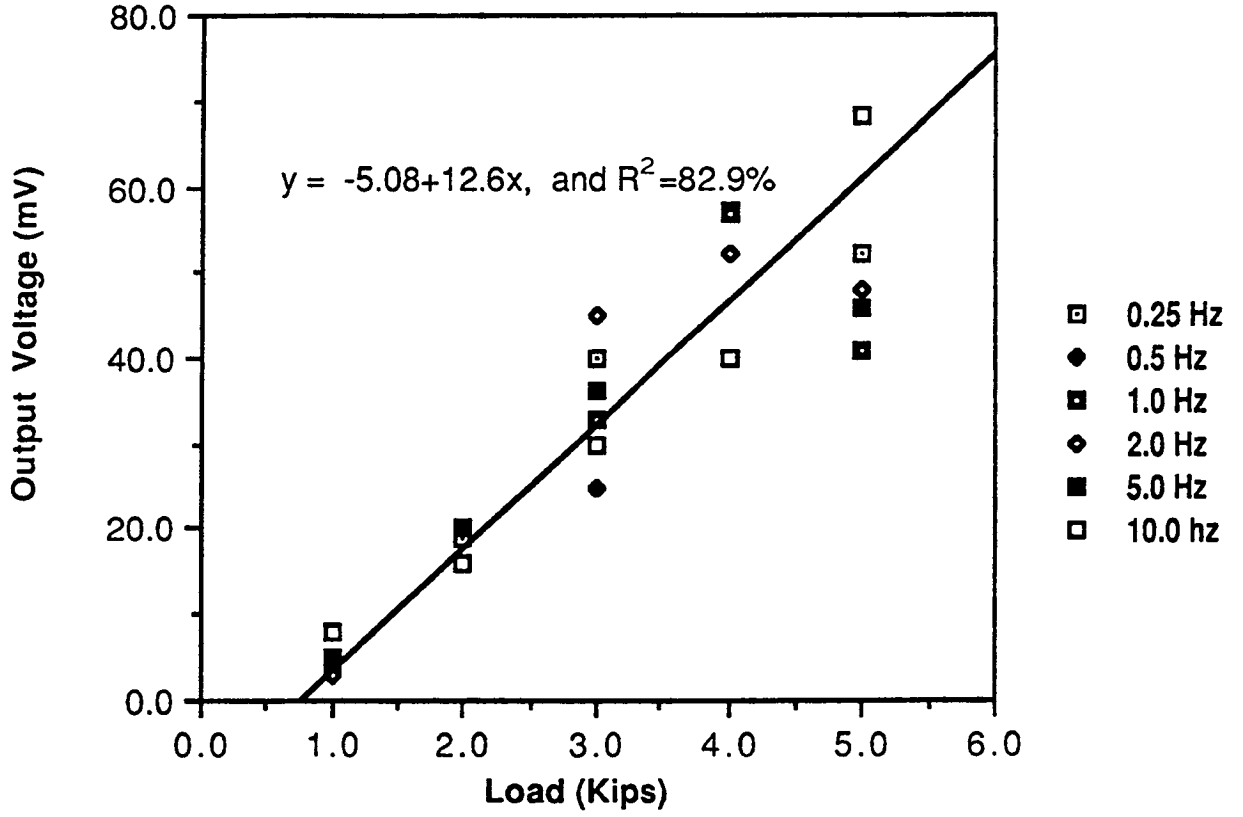

Fig. 5-6 Linear regression of experimental data for piezoelectric sensor at varying frequencies of applied load.

6

Concluding Remarks

The main purpose of this project was to study the feasibility of designing, developing, and implementing a low cost fiber-optic WIM sensor as a possible replacement for piezoelectric WIM sensors. A prototype fiber-optic pressure sensor was designed, manufactured and tested. The sensor consists of a fiber-optic displacement sensor, an expandable hose filled with fluid, an elastomer pad housing the expandable hose, and a stainless-steel diaphragm. The prototype sensor was tested under an MTS loading cell. The performance of the sensor under various loads and different application frequencies was evaluated. Similar tests were performed on a piezoelectric sensor used in WIM systems.

The output signals from each of the two sensors under varying load magnitudes and frequencies were compared. Among the performance attributes considered were (1) the correlation between the applied load and the output voltage signal received, (2) the shape of the output waveforms, and (3) the variation of the output signal with application frequency of the load. In the latter two categories, the optical sensor proved to be superior to the conventional piezoelectric sensor. In the first category, both sensors displayed a fairly linear trend between the magnitude of the output signal and the load applied.

While laboratory tests on the fiber-optics sensor have yielded promising results, the sensor is certainly not ready for field implementation. A number of issues must be addressed prior to the implementation phase. The sensor performance characteristics can be optimized through revisions in the design of the various sensor components. The sensor performance needs to be monitored in the field and under actual traffic conditions. Other aspects such as calibration, signal processing, power utilization, and integration into existing vehicle monitoring and classification systems must also be undertaken.

Among the design improvements to be probed is the choice of fluid used to fill the tube to be stretched across the road. The function of the fluid is to transfer the applied pressure to the displacement diaphragm. The transfer of pressure, in any fluid medium, must be fairly instantaneous and without much pressure loss; therefore, a fairly incompressible fluid must be used. The degree of instantaneity required is, of course, a function of how frequently pressure is applied. In the lab tests, water was found to perform satisfactorily for frequencies up to 10 Hz. For the usual range of operating speeds and axle spacings, frequencies exceeding 10 Hz are rarely experienced. The sensitivity of water to temperature, however, makes it unsuitable for field applications. Brake fluid is a potentially good replacement, as it is incompressible and considerably less temperature sensitive than water. It is, however, not an ideal fluid in case of a ruptured tube and spillage into the pavement surface. The search for the fluid to be used should also focus on the chemical properties of the fluid, specifically its interaction with pavement materials and its effect on skid resistance characteristics of the pavement surface.

The rubber padding must also undergo improvements in design. Specifically, different mix ratios of the Flexane resin and curing agents used in the laboratory prototype must be evaluated. The evaluation criteria should consider those characteristics of the rubber padding desirable under operational field conditions. Among them, the padding must be perfectly elastic for the type of wheel loads expected. Yet, the rubber used must be of a hardness to prevent deflections so great as to completely close off the highly flexible hose embedded in the padding. The shape of the padding should be of concern. A semi-cylindrical padding was used in the laboratory tests. However, the bulge introduced on the pavement surface by a semi-cylindrical pad is likely to amplify the undesirable vertical motion of wheels and, thus, the dynamic loading conditions. The padding to be used in the field must have a thin aerodynamic shape, yet be thick, enough to provide a suitable cushion for the embedded 0.25-in diameter flexible hose. Whether or not a smaller diameter inner hose can be used should also be addressed. The latter, however, is a function of the rubber padding. Therefore, an optimum design for field conditions should be reached in terms of the elasticity, hardness, temperature sensitivity, shape, and thickness of the rubber padding as well as the diameter of the inner hose.

Upon design improvements which condition the sensor for field applications, a number of field tests must be conducted. The sensor must be tested for a variety of known axle load and combinations. One possibility is to set up the sensor upstream or downstream of static weigh stations on the highway. This would provide data on a variety of axle configurations and loads. However, it would require coordination with and cooperation of state highway agencies. Furthermore, unless many sites are monitored, insignificant variation in speeds can be obtained. An alternative

which may prove more advantageous is to conduct the test on proving grounds using one or more trucks of known weight passing over the sensor at different speeds. The truck weight can be easily varied by using, for example, a water tanker truck filled with sand that dumps a known volume of its load after each set of runs.

Another important aspect of field operations is that of lane discrimination. If the tube is stretched across the entire roadway width, then near simultaneous signals can be received from two or more vehicles traveling shoulder-to-shoulder in adjacent lanes. While this may not be critical if only the total individual axle loads were sought, it would be impossible to determine the gross weights or the distribution of axle and vehicle weights by lane.

In making volume counts using pneumatic tubes, lane discrimination is achieved through multi-installation of counter tubes. In a two-lane case, for example, depending on the roadway geometry either a separate tube is stretched across each lane or one tube is across the entire roadway width and a second one across the right or the left lane. Multilane installations may not be a feasible approach in the case of proposed optical WIM sensor, since each sensor has an air-bleed valve at each of the two ends. It is, therefore, difficult, unlike the volume counters, to terminate and clamp down a WIM tube halfway across the pavement area. Alternatives are to modify the design, to alleviate the need for two air-bleed valves, or devise a mechanism to close down the inner tube at intermediate points so as to only receive signals emanating from a specific lane.

The lane discrimination problem should be studied in conjunction with integrating the optical WIM sensor into the existing vehicle classification systems. The sensors can easily replace axle detectors in the existing classification systems. They also provide an additional piece of data, namely the axle weight, thus making it unlikely to classify, for example, a six-axle truck as three separate vehicles. On the other hand, the lane discriminator logic of the vehicle classification system can help determine the gross vehicle weights and distribution of axle loads by lane.

Finally, a number of issues relating to signal processing must be addressed. Given the operational characteristics of the optical displacement sensor, effective means of filtering the noise and amplifying the signal must be devised. Shape, duration, and peak voltage of the signals must be correlated to the axle weight and loading frequency. Necessary calibrations can be then carried out. Efficient means of data transmission and storage must also be developed. Among the factors to be considered are the degree of immunity from EMI and electromagnetic pulses, power requirements for signal processing, and degree of compatibility with signal processing and data transmission procedures in the existing vehicle classification and WIM systems.

In short, the proposed fiber-optics displacement sensor is highly promising.

Extensive laboratory tests have proven the concept to be operational and, in comparison to piezoelectric cables, potentially much more accurate. The cost is also considerably lower, namely, under $1,000 per complete sensor system as compared to the piezoelectric sensor with a price tag of at least $2,500 per lane. Additional savings are realized in sensor installation, that unlike other WIM sensors, requires no in-pavement installation or surface affixation.

References

1. McCall, B.M., *"Status Report of Federal Highway Administration Demonstration Project,"* Presented at the 66th Annual Meeting of the Transportation Research Board, Washington, D.C., January 1987.

2. *"Concepts, Advantages, and Applications of WIM Systems"*. National Weigh-In-Motion Conference, U.S. Department of Transportation, FHWA and Colorado Department of Highways, Denver, Colo., July 11-15, 1983.

3. Al-Rashid, N.I., C.E. Lee and W.P. Dawkins. *"A Theoretical and Experimental Study of Dynamic Highway Loading,"* Report No. 108-1F. Center for Transportation Research, The University of Texas at Austin, 1972.

4. Lee, C.E., B. Izadmehr and R.B. Machemehl. *"Demonstration of Weigh-In-Motion Systems for Data Collection and Enforcement,"* Report No. 557-1F. Center for Transportation Research, The University of Texas at Austin, December 1985.

5. Papagiannkis, A.T., W.A. Phang, J.H.F. Woodrooffe, A.T. Bergen, and R.C.G. Haas. *"Accuracy of Weigh-In-Motion Scales and piezoelectric cables,"* Paper 880449. presented at the 68th Annual Meeting of the Transportation Research Board, January 1989.

6. Izadmehr, B. and C.E. Lee. *"Accuracy and Tolerances of WIM Systems,"* Presented at the 66th Annual Meeting of the Transportation Research Board, Washington, D.C., January 1987.

7. Sommerville, F. and P. Davies, *"Low Cost WIM with Piezo Cables,"* Presented at the 67th Annual Meeting of the Transportation Research Board, Washington, D.C., January 1988.

8. Davies, P., F.K. Sommerville, M. Bettison, and D.R. Salter, *"Fundamental Properties of Piezo-electric Cable"*, Report to the Transport and Road Research Laboratory, Phases I-IV, University of Nothingham, 1981-1985.

9. Giallorenzi, T.G., J.A. Bucaro, A. Dandridge, G.H. Siegel, Jr., J.H. Cole, S.C. Rashleigh and R.G. Priest. *"Optical Fiber Sensor Technology,"* IEEE Journal of Quantum Electronics, Vol. QE-18, April 1982, pp.626-665.

10. Dakin, J.P. *"Optical Fiber Sensors; Principles and Applications,"* SPIE, Vol. 374, April 1983, pp. 173-183.

11. Culshaw, B. *"Optical Fiber Sensing and Signal Processing"* , Peter Peregrinus Ltd., London, 1984.

12. Nakayama, T. *"Optical Sensing Technologies by Multimode Fibers,"* SPIE, Vol. 478, 1984, pp. 19-26.

13. Davis, C.M. *"Fiber-Optic Sensors: an Overview,"* Optical Engineering, Vol. 24, March-April 1985, pp. 347-351.

14. McMillan, J.L. and S.C. Robertson. *"Single-Mode Optical Fiber Sensors,"* GEC Journal of Research, Vol. 2, 1984, pp. 119-124.

15. Safaai-Jazi, A., and R.O. Claus. *" Synthesis of Interference Patterns in Few-Mode Optical Fibers,"* SPIE proceedings on Fiber Optic Smart Structures and Skins, Vol. 986, pp. 180-185, 1989.

16. Lagakos, N., P. Macedo, T. Litovitz, R. Mohr, and R. Meister. *"Fiber Optic Displacement Sensor,"* in Physics of Fibers, Vol. 2, Advances in Ceramics , B. Bendow and S.S. Mitra, Eds. Columbus, Ohio: Amer. Ceramic Society, pp. 539-544, 1981.

17. Personick, S.D. Fiber Optics, Plenum press, New York, 1985.

18. Palais, J.C. Fiber Optics Communications, Prentice-Hall, Englewood Cliffs, N.J., 1988.

19. Davies P. and F.K. Sommerville. *"Low-Cost WIM: The Way Forward,"* Presented at the 2nd National WIM Conference, Atlanta, Ga, 1985.

20. Auld, B.A. Acoustic Waves in Solids, John Wiley and Sons, New York, 1973.

21. Mactavish, D. and D.L. Neumann. *"Highway Performance Monitoring System-Vehicle Classification Case Study,"* ,FHWA , Washington, D.C., August 1982.

SHRP-IDEA Advisory Committee

Mark Yancey, *chairman*
Texas Department of Transportation

William G. Agnew
General Motors Research (retired)

Raymond Decker
University Science Partners, Inc.

Barry J. Dempsey
University of Illinois

Serge Gratch
GMI Engineering and Management Institute

Arun M. Shirole
New York State Department of Transportation

Earl C. Shirley
California Department of Transportation

Richard N. Wright
National Institute of Standards and Technology

Liaisons

Tom Christison
Alberta Research Council

Lawrence L. Smith
Florida Department of Transportation

Edwin W. Hauser
Arizona State University

Roy S. Hodgson
Consultant

Thomas J. Pasko, Jr.
Federal Highway Administration

Robert Spicher
Transportation Research Board